PARAMETRIC SMALL-SIGNAL MODELING OF GRID FORMING AND GRID FOLLOWING INVERTERS IN 100% RENEWABLE BASED GRID

A Dissertation
Presented to
The Academic Faculty

By

Araz B Karimi

In Partial Fulfillment
of the Requirements for the Degree
Master of Science in the
Department of Electrical and Computer Engineering

Georgia Institute of Technology

December 2022

PARAMETRIC SMALL-SIGNAL MODELING OF GRID FORMING AND GRID FOLLOWING INVERTERS IN 100% RENEWABLE BASED GRID

Thesis committee:

Dr. Maryam Saeedifard
Electrical and Computer Engineering
Georgia Institute of Technology

Dr. Deepakraj M Divan
Electrical and Computer Engineering
Georgia Institute of Technology

Dr. Santiago Grijalva
Electrical and Computer Engineering
Georgia Institute of Technology

Date approved: August 26, 2022

ACKNOWLEDGMENTS

I would like to thank the members of my thesis committee for their help in the preparation of this work – Dr. Maryam Saeedifard, Who gave me invaluable advice and guidance during the project and who helped me have a better understanding of complex topics in this work. Dr. Grijalva, Dr. Deepak Divan, and Dr. Meliopoulos, whose advice inspired me to improve my work.

Special thanks are due to my wife, who made this work possible with her support and understanding. This work couldn't be done without her inextinguishable encouragement.

The author gratefully acknowledges the support for this work offered by the Center for Distributed Energy (CDE) at Georgia Tech and by the Power System Engineering Research Center (PSERC), which funded this research.

TABLE OF CONTENTS

LIST OF TABLES

LIST OF FIGURES

LIST OF ACRONYMS

EMT Electromagnetic Transient

GFL Grid Following Inverter

GFM Grid Forming Inverter

MMC Modular Multilevel Converter

PLL Phase-Locked Loop

PSC Power Synchronization Control

PV Photovoltaic

PWM Pulse-Width Modulation

RMS Root Mean Square

Syn Synchronvertor

VIL Virtual Inertia

WECC Western Electricity Coordinating Council

SUMMARY

Due to the concerns about global warming, its critical environmental consequences, and the availability of fossil fuels in the near future, several power systems in the world will aim to become 100 % renewable-energy-based. This future grid with 100% inverter-based generation is structurally different in response to various phenomena. Therefore accurate modeling of inverters in this new structure is a crucial task. This thesis introduces a new parametric high-fidelity small-signal model of the Grid Forming Inverter (GFM) and Grid Following Inverter (GFL). Different control strategies for GFM, such as virtual-inertia-based, synchronvertor, power synchronization control, and droop are considered. New control loops are introduced in which the measured signals are related to the angle generation block in GFMs. To obtain the comprehensive model, first, nonlinear blocks (power measurement, DC-side dynamics, dq/abc frame transforms, Phase-Locked Loop (PLL), and GFL droop) are linearized, and inverter block diagrams are converted to matrix form subsequently. Then, a set of first-order algebraic equations are formed based on the matrix equations and computationally solved in MATLAB. After derivation of output admittance in matrix form, derived block components are replaced to form four transfer functions that define the dynamics of the inverter. The results show the significant dependency of inverter stability on a steady-state angle obtained via load flow and current loop proportional gain. Therefore a stability margin for steady-state angle is derived, which is analogous to the angle stability of synchronous generators. The synchronvertor controller shows a very complex transfer function with the most unstable and challenging behavior among the rest of the inverters.

Keywords:- Grid Forming Inverters - Inverter Modeling - Inter-Area Oscillations

CHAPTER 1
INTRODUCTION AND BACKGROUND

1.1 The 100% Renewable Grids: The Trend and Emerging Challenges

As a result of the concerns over worldwide climate change and growing demands for electricity, the integration of significant amounts of renewable energy into power systems has gained increasing traction. In Europe, the US, China, and Australia, legislative acts have been enforced to increase renewable energy usage. For example, Denmark aims to achieve 100% renewable energy supply by 2050, eliminating the dependency on fossil fuels. In the US, some states have mandated carbon-free electricity for their future electricity grids, e.g., California has mandated 100% renewable energy supply by 2045, while Minnesota has passed laws to move to a fully renewable energy supply by 2050. These trends have led to the integration of massive wind and Photovoltaic (PV) plants up to several hundred megawatts to be connected to the power grid in certain regions. [1].

The primary renewable energy resources used in the power system, which are solar and wind-based, use inverter-based integration due to their intermittent power generation and lack of mechanical power. Therefore, to fulfill the mentioned goals, the inverter-based power generation may be dominant and force synchronous generators to be obsolete. This structural change may cause problems with power system strength, dynamics, stability, and response to a wide variety of phenomena. These emerging problems require modification of power system apparatus, especially inverters, to maintain their reliable performance in terms of low system inertia, fault-ride-through, response to grid phase shift, post fault recovery, inter-area oscillation damping, black start, current limitations during short-circuits, and frequency and voltage support. Therefore, different approaches are taken towards imposing new standards and modifying inverters to make the system compatible with this new

structural change.

1.2 Significance of the Technical Problem

Unlike the synchronous generator-based power systems with a well-established theoretical explanation of dynamics, stability, and power system strength, the theoretical analysis of inverter-based AC grids, especially for the large, primary, and high-voltage systems, remains unexamined. The primary prerequisite for developing such theoretical explanations is the exact inverter modeling in the power systems. This modeling should be comprehensive and include all phenomena that can happen in a system. However, to simplify the analysis, the modeling can be divided into pieces where each explains a set of different phenomena. This phenomena can be classified based on different factors such as magnitude and frequency. One significant phenomenon in the power system operation that may require further study in the inverter-based grid is the inter-area oscillation, which can be classified into the small-signal and low-frequency scope. The most crucial prerequisite for studying the inverter-based grid in small-signal and low-frequency is the individual inverter modeling in the small-signal.

1.3 Summary of the Proposed Method

In this study, an approach has been developed toward modeling the inverter in the small signal analysis, in which the parametric model of the inverter is developed using a matrix formulation and linearization of specific blocks in small-signal by using a computational algebraic equation solver. Most inverter strategies, such as different GFMs and GFLs, are covered in the modeling. In order to fully understand the inverter response to the undergoing phenomena, an accurate inverter model is necessary. This model should include large and small signals to cover all the phenomena. However, in this thesis, which is a part of an ongoing research project, only the exact small-signal model for the newest inverter control strategies and different operation points are parametrically derived. This is to first ensure

the nonlinear system's stability on the operation point and second to pave the way to the capture and reduction of the inter-area oscillations.

1.4 Thesis Structure

In the rest of the thesis, first, previous inverter modeling approaches are discussed in chapter 2. In chapter 3 the matrix form inverter modeling approach is explained, and a small-signal equation for each inverter block is theoretically derived. These blocks are computationally solved in chapter 4 and the resultant equivalent impedance/admittance transfer functions are derived and presented. In chapter 5, first GFMs are compared in terms of the number of the poles and frequency response, and then, parameter sensitivity analyses are performed to highlight the importance of specific parameters. Finally, chapter 6 concludes the thesis and sheds light on future research.

CHAPTER 2

LITERATURE REVIEW

In this chapter, the first existing inverter modeling approaches are presented, and then the candidate model, i.e., eigenvalue-based literature, is elaborated on in more detail.

2.1 Power System Phenomena Classification

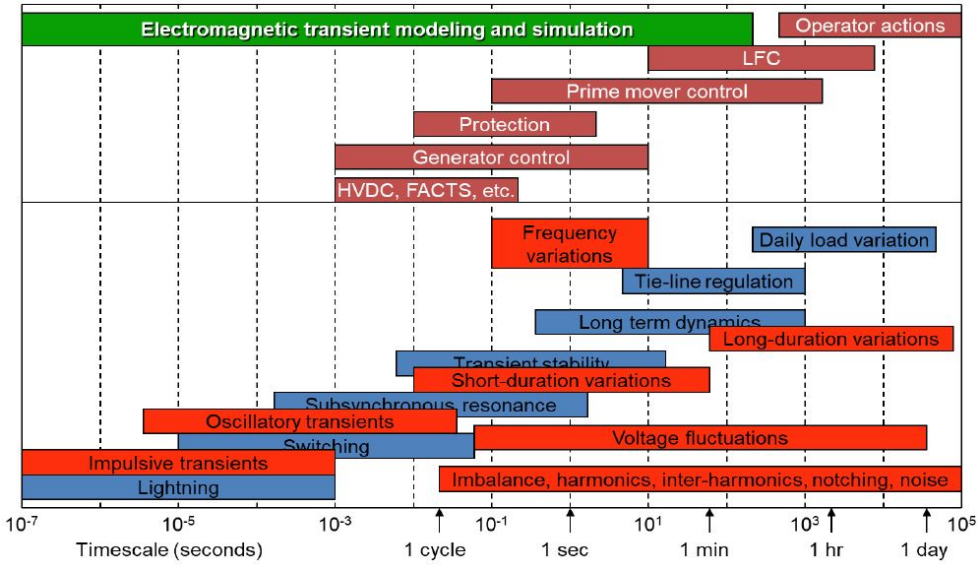

Figure 2.1: Power system phenomena and required accuracy of modeling.[2]

Figure 2.1 shows the different power system phenomena and their time scales. In power system modeling and study it is very important to chose a time scale that captures the desired phenomena and meanwhile is computationally efficient. Two main types of power system modeling are Electromagnetic Transient (EMT) and Root Mean Square (RMS). Other modeling approaches are categorized within one of the aforementioned modeling methods.

2.2 EMT-Based Model

2.2.1 Dommel's Method

EMT model, the most exact model of an electrical device, considers time domain differential equations of all circuit elements and solves them in the time domain. The first computationally feasible approach was introduced by Domell in the late 60s [3] [4]. In Dommel's method, every linear and nonlinear circuit element is modeled as a current source in parallel with a linear circuit element within a specific time interval. Dommel's method is still being used in software tools such as PSCAD (EMTDC) and EMTP. These methods are computationally time-consuming and must be used when a very high-frequency phenomenon needs to be captured or when the maximum short circuit current caused by a high-frequency component in the waveform needs to be measured.

2.2.2 Piece-wise Average Model

One of the significant causes of nonlinearity in power system components is semiconductor devices that exist in all inverters. Including the exact model of these switches makes simulation time enormously long. To accelerate EMT simulations of the PWM converters, a novel algorithm was proposed later, which integrates an improved averaged model of Pulse-Width Modulation (PWM) inverters into the EMT. [5] The performance of this method is acceptable in studying specific switching and short circuits that include PWM inverters. However, this average model integration makes the simulation inaccurate for faster phenomena such as lightnings.

2.2.3 Dynamic Phasor Modeling

Dynamic phasors are also another method that tries to make a bridge between EMT and RMS methods. For example, a dynamic phasor model of a Modular Multilevel Converter (MMC) with extended the frequency range for direct interfacing to an EMT simulator is

introduced in [6] and [7]. The internal dynamics of the MMC are modeled considering dominant harmonic components of each variable. To model the external dynamics of the converter, a novel construct referred to as a base-frequency is employed, which allows to capture and model any number of frequency components of external variables without any significant increase in computational burden [6].

2.3 RMS-Based Models

Because the slower phenomena can be accurately captured with a less complicated method, using time-consuming EMT modeling for every phenomenon seems unnecessary. Therefore, methods such as RMS with lesser computational burdens are developed to tackle the speed problem. RMS models are models that use the phasor model of components and are lighter than EMT models. RMS models are widely used in software tools such as MATLAB Simulink and DIgSILENT Powerfactory. This modeling approach is a basis for some inverter models, as follows:

2.3.1 Average Model

The average model linearizes the inverter switching by considering an average value of two on and off cycles. [8] This approximation enables RMS to include inverters in the simulation. The average model is widely used in inverter design, stability, and control and is a basis for other inverter RMS models.

2.3.2 Generic Models

Generic models comes as a package and include most of control block diagrams and circuit components for inverters. Generic models are developed by standards in order to make a general widely used model of inverters, so that can be used as benchmark in industry and academia. For example Generic models of Western Electricity Coordinating Council (WECC) are presented and validated for wind and solar energy integration [9]. These

models have their own limitations and flexibility problems and may not be suitable for particular phenomena or particular inverter functionality. In addition, because standards provide them, they are being updated slowly, and new technologies cannot be implemented readily in generic models.

2.3.3 Eigenvalue Based

In order to capture certain power system phenomena such as inter-area oscillations and ensure small-signal stability in conventional systems, eigenvalue analysis is a well-established method [10]. However, implementing this method for inverter-based systems is a novel concept. In [11] a modal analysis is made for a coupled GFM and GFL using a global eigenvalue analysis. The results are accurate for a two-inverter system, but the method lacks modularity and scalability. Unified impedance models, however, solve this problem. In [12] and [13], the complex transfer function formulation, which is the benchmark of small-signal studies, is introduced. A complete model is later introduced in [13] In [14], an additional dq/abc transform block is added to the small-signal model. Finally, in [15], a small-signal model for GFM is introduced, which is limited to the Virtual Inertia (VIL) GFMs. Therefore, an analysis of the other GFM topologies alongside with GFLs is still unexamined. Besides, in the literature mentioned, GFMs are considered a constant angle device, and the GFM angle generation loop is not considered.

2.4 Section Summary

This chapter provided a literature review on the modeling of inverters. Among different methods, eigenvalue (small-signal) based methods built based on the average switch model are more suitable for inter-area oscillation studies. Besides the valuable literature on the inverter small-signal concept, the small-signal model is the most efficient method for studying oscillations for different inverter GFM topologies. Steady-state angle difference, DC side dynamics, and LCL filter effect are not considered holistically. In this thesis, the focus

is to include different inverter strategies and also include all possible block diagrams comprehensively. Later, the explicit small-signal parametric equations are derived numerically to be used in a scalable approach.

CHAPTER 3
METHODOLOGY

This chapter first explains the theory and assumptions behind small-signal analysis of the inverters and then elaborates on the mathematical linearization and derivation of the small-signal matrix form of each function in an inverter. Finally, it summarizes the full small-signal model by presenting a matrix form block diagram representation.

3.1 Background Theory and Procedure

In the future 100% inverter-based power system, system inertia will be low; therefore, the inter-area oscillations may remain undamped for a long time. This work in the first phase is to build comprehensive small-signal model of the inverter-based resources, which would be used to analyze system stability and solve the problems of the inter-area oscillation damping. The general approach for inter-area oscillation can be summarized in three steps.

- Derivation of equivalent small-signal output inductance model for a single inverter
- Order reduction of the resultant equivalent small-signal output inductance to enable computational and visual inter-area oscillation analysis.
- Integration of order reduced equivalent small-signal output inductance model to derive small-signal modes and performing tuning to improve the overall system damping.

In this thesis, the focus is on the modeling part of the mentioned procedure. However, precautions are taken to make it readily available for eigenvalue analysis and model reduction. Therefore, the equivalent impedance/admittance matrix approach has been used instead of the commonly used state-space model. This approach makes the inverter level or-

der reduction significantly easier. In addition, it allows the different elements of the circuit to be added to multiple inverter sets in a modular manner.

Certain assumptions are made in order to make the system able to rely on small-signal model in specific phenomena. For example, all protection systems, such as current limiting and fault ride-through controls, are neglected during a small-signal oscillation. In addition, because the study is on the transmission and generation side, the anti-islanding protections which specific for distribution inverters are not considered. Dynamics of the input energy source is neglected and considered slow. Therefore, the DC side is considered as an equivalent capacitor and a constant input current. It is also assumed that if a perturbation happens in the magnitude of PWM input, the output perturbation is not affected by the high-frequency terms, and therefore switching frequencies can be neglected. It is assumed that the V_{ref} and θ_{ref} are determined by the optimal power flow studies at the system level, which is slower than system dynamics.

It needs to be mentioned that the frequency perturbation is only considered as a dependent variable to output voltages or currents rather than an independent variable, and no independent changes in the frequency are assumed.

The main theory behind equivalent impedance/admittance modeling is that the poles of the equivalent impedance/admittance transfer functions are identical to the eigenvalues of the inverter.

Because the inverters are considered to be three-phase and balanced, they can be transformed into dq frame for control purposes. For example, voltage, current, and modulation index that are inherently complex signals will be shown as a 2×1 matrix containing both d and q axis components. System signals such as angle and DC voltage are converted into the matrix format to obtain a generalized formulation for each block. Because of the couplings between d and q frames on the controller side, the corresponding impedance/admittance or the block equivalent gain must be a 2×2 matrix. For example, the conversion for impedance formulation will become:

$$\Delta V = Z_{out}\Delta I \tag{3.1}$$

where:

$$Z_{out} = \begin{bmatrix} Z_{out}^{dd} & Z_{out}^{dq} \\ Z_{out}^{qd} & Z_{out}^{qq} \end{bmatrix} \tag{3.2}$$

and

$$\Delta V = \begin{bmatrix} V_d \\ V_q \end{bmatrix} \tag{3.3}$$

and

$$\Delta I = \begin{bmatrix} I_d \\ I_q \end{bmatrix} \tag{3.4}$$

where:

$$\begin{aligned} \Delta V_d &= Z_{out}^{dd}\Delta I_d + Z_{out}^{dq}\Delta I_q \\ \Delta V_q &= Z_{out}^{qd}\Delta I_d + Z_{out}^{qq}\Delta I_q \end{aligned} \tag{3.5}$$

3.2 Small-Signal Approximation of Inverters

In this section, small-signal formulation of each part in inverter model is presented based on the theory mentioned in section 3.1

The prime-suffixed variables denotes the measured variables in the local dq frame. The difference between local and global dq frames which are explicitly shown in sub-section 3.2.8.

3.2.1 Output Filter

The L filert

For L filter the dq matrix form equation is:

$$\Delta V_o - U = \begin{bmatrix} sL & -L\omega \\ L\omega & sL \end{bmatrix} \Delta I \tag{3.6}$$

where L is the inductance of the inductor, s is the Laplace variable and the ω is the system frequency. The variables are ΔV_o, output voltage, ΔU, inverter's voltage, and ΔI, the inverter's current perturbations. Equation 3.6 can be written in matrix form as:

$$\Delta V_o - U_c = \mathbf{Z_L} \Delta I_o \tag{3.7}$$

where $\mathbf{Z_L}$ is the inductor's impedance in the matrix form.

The LCL filert

For LCL filter the dq matrix form equation is:

$$\Delta V_o - V_c = \begin{bmatrix} sL_2 & -L_2\omega \\ L_2\omega & sL_2 \end{bmatrix} \Delta I_o \tag{3.8}$$

$$\Delta I_o - \Delta I = \begin{bmatrix} sC & -C\omega \\ C\omega & sC \end{bmatrix} \Delta V_c \tag{3.9}$$

$$\Delta U - \Delta V_c = \begin{bmatrix} sL_1 & -L_1\omega \\ L_1\omega & sL_1 \end{bmatrix} \Delta I \tag{3.10}$$

which can be written in matrix form as:

$$\Delta V_o - V_c = \mathbf{Z_{L2}} \Delta I_o \tag{3.11}$$

$$\Delta I_o - \Delta I = \mathbf{Z_c} \Delta V_c \tag{3.12}$$

$$\Delta U - \Delta V_c = \mathbf{Z_{L1}} \Delta I \tag{3.13}$$

3.2.2 PWM

In reality, the PWM block is the inverter itself that takes the input from the controls and converts it into a duty cycle for the switching device. This switching of DC voltage with varying duty cycles makes a controlled output AC voltage after low-pass filtering. The assumption here is that the high frequency is neglected in the small-signal, and the average model for switching devices is inherently used. The main equation for the PWM block is:

$$U = INV * V_{DC} D \tag{3.14}$$

where D is the modulation index and U is the output voltage. Both D and U are considered in dq frame as $D = \begin{bmatrix} D_d \\ D_q \end{bmatrix}$ and $U = \begin{bmatrix} U_d \\ U_q \end{bmatrix}$. The Equation 3.14 is nonlinear and must be linearized for small-signal analysis. The $*$ operator denotes simple matrix multiplication.

$$U + \Delta U = INV * (V_{DC} + \Delta V_{DC})(D + \Delta D) \tag{3.15}$$

where $INV = \begin{bmatrix} \frac{1-0.5T_{del}s}{1+0.5T_{del}s} & 0 \\ 0 & \frac{1-0.5T_{del}s}{1+0.5T_{del}s} \end{bmatrix}$ is the switching delay transfer function in the matrix form and

$$U + \Delta U = INV * ((V_{DC})(D) + (V_{DC})(\Delta D) + (\Delta V_{DC})(D) + (\Delta V_{DC})(\Delta D)) \tag{3.16}$$

By neglecting steady-state and double incremental terms we obtain:

$$\Delta U = INV * ((V_{DC})(\Delta D) + (\Delta V_{DC})(D)) \tag{3.17}$$

Finally,

$$\Delta U = Delv * \Delta D + Deld * \Delta V_{DC} \tag{3.18}$$

in which $Delv = INV * V_{DC}$ and $Deld = INV * D$

3.2.3 Current Loop

Inner current loop is a linear block that controls the input of PWM with its reference current and can be seen in Equation 3.19.

$$\Delta D' = \begin{bmatrix} PI_c & 0 \\ 0 & PI_c \end{bmatrix} (\Delta I_{ref} - \Delta I') + \begin{bmatrix} 0 & -L_1\omega \\ L_1\omega & 0 \end{bmatrix} \Delta I' + \begin{bmatrix} fv & 0 \\ 0 & fv \end{bmatrix} V_c' \tag{3.19}$$

and the final matrix form equation can be derived as:

$$\Delta D' = PIC(\Delta I_{ref} - \Delta I') + L1w * \Delta I' + FV * V_c' \tag{3.20}$$

3.2.4 Voltage/Power Loop

Power Loop in GFL: Power loop is used in GFL to provide a constant active and reactive power:

$$\Delta I_{ref} = \begin{bmatrix} PI_p & 0 \\ 0 & PI_q \end{bmatrix} (\Delta S_{ref} - \Delta S) \tag{3.21}$$

which can be rewritten in the matrix form as:

$$\Delta I_{ref} = PIS * (\Delta S_{ref} - \Delta S) \tag{3.22}$$

Voltage Loop in GFM: Voltage loop is used in GFM in order to control the voltage:

$$\Delta I_{ref} = \begin{bmatrix} PI_v & 0 \\ 0 & PI_v \end{bmatrix} (\Delta V_{ref} - \Delta V_c') + \begin{bmatrix} 0 & -C\omega \\ C\omega & 0 \end{bmatrix} \Delta V_c' + \begin{bmatrix} fc & 0 \\ 0 & fc \end{bmatrix} \Delta I' \quad (3.23)$$

By assuming that the $V_{ref} = constant$, Equation 3.23 can be reduce to:

$$\Delta I_{ref} = - \begin{bmatrix} PI_v & 0 \\ 0 & PI_v \end{bmatrix} \Delta V_c' + \begin{bmatrix} 0 & -C\omega \\ C\omega & 0 \end{bmatrix} \Delta V_c' + \begin{bmatrix} fc & 0 \\ 0 & fc \end{bmatrix} \Delta I' \quad (3.24)$$

Therefore, The matrix form of Equation 3.23 is:

$$\Delta I_{ref} = -PIV * \Delta V_c' + Cw * \Delta V_c' + F_{II} * \Delta I' \quad (3.25)$$

3.2.5 Power Measurement

Power measurements in terms of I_d', I_q', V_d', and V_q' are:

$$P = \frac{\omega_c}{s + \omega_c}(V_d' I_d' + V_q' I_q') \quad (3.26)$$

$$Q = \frac{\omega_c}{s + \omega_c}(V_q' I_d' - V_d' I_q') \quad (3.27)$$

where $pfilter = \frac{\omega_c}{s+\omega_c}$ is a low-pass filter for measurement. This is a nonlinear block, and it needs to be linearized in order to be used in small-signal analysis. The linearization has been done as follows:

$$P + \Delta P = pfilter((V_d' + \Delta V_d')(I_d' + \Delta I_d') + (V_q' + \Delta V_q')(I_q' + \Delta I_q')) \quad (3.28)$$

$$Q + \Delta Q = pfilter((V'_q + \Delta V'_q)(I'_d + \Delta I'_d) - (V'_d + \Delta V'_d)(I'_q + \Delta I'_q)) \tag{3.29}$$

eqs. (3.28) and (3.29) can be elaborated as:

$$\begin{aligned} P + \Delta P = pfilter((V'_d)(I'_d) + (V'_q)(I'_q) + (\Delta V'_d)(I'_d) + (\Delta V'_q)(I'_q) + (V'_d)(\Delta I'_d) \\ +(V'_q)(\Delta I'_q) + (\Delta V'_d)(\Delta I'_d) + (\Delta V'_q)(\Delta I'_q)) \end{aligned} \tag{3.30}$$

$$\begin{aligned} Q + \Delta Q = pfilter((V'_q)(I'_d) - (V'_d)(I'_q) + (\Delta V'_q)(I'_d) - (\Delta V'_d)(I'_q) + (V'_q)(\Delta I'_d) \\ -(V'_d)(\Delta I'_q) + (\Delta V'_q)(\Delta I'_d) - (\Delta V'_d)(\Delta I'_q)) \end{aligned} \tag{3.31}$$

If the large signal and double incremental terms are dropped, the equation will become:

$$\Delta P' = pfilter((I'_d)(\Delta V'_d) + (I'_q)(\Delta V'_q) + (V'_d)(\Delta I'_d) + (V'_q)(\Delta I'_q)) \tag{3.32}$$

$$\Delta Q' = pfilter((I'_d)(\Delta V'_q) - (I'_q)(\Delta V'_d) + (V'_q)(\Delta I'_d) - (V'_d)(\Delta I'_q)) \tag{3.33}$$

which can be rewritten as:

$$\Delta P' = pfilter(\begin{bmatrix} I'_d & I'_q \end{bmatrix} \begin{bmatrix} \Delta V'_d \\ \Delta V'_q \end{bmatrix} + \begin{bmatrix} V'_d & V'_q \end{bmatrix} \begin{bmatrix} \Delta I'_d \\ \Delta I'_q \end{bmatrix}) \tag{3.34}$$

$$\Delta Q' = pfilter(\begin{bmatrix} -I'_q & I'_d \end{bmatrix} \begin{bmatrix} \Delta V'_d \\ \Delta V'_q \end{bmatrix} + \begin{bmatrix} V'_q & -V'_d \end{bmatrix} \begin{bmatrix} \Delta I'_d \\ \Delta I'_q \end{bmatrix}) \tag{3.35}$$

and finally,

$$\Delta S = \begin{bmatrix} pfilter & 0 \\ 0 & pfilter \end{bmatrix} \left(\begin{bmatrix} I'_d & I'_q \\ -I'_q & I'_d \end{bmatrix} \begin{bmatrix} \Delta V'_d \\ \Delta V'_q \end{bmatrix} + \begin{bmatrix} V'_d & V'_q \\ V'_q & -V'_d \end{bmatrix} \begin{bmatrix} \Delta I'_d \\ \Delta I'_q \end{bmatrix} \right) \tag{3.36}$$

We assume $Io = \begin{bmatrix} I'_d & I'_q \\ -I'_q & I'_d \end{bmatrix}$, $Vo = \begin{bmatrix} V'_d & V'_q \\ V'_q & -V'_d \end{bmatrix}$ and $Pfilter = \begin{bmatrix} pfilter & 0 \\ 0 & pfilter \end{bmatrix}$ to derive the matrix form:

$$\Delta S = Pfilter(Io\Delta V' + Vo\Delta I') \tag{3.37}$$

3.2.6 DC-side Dynamics

Based on the law of conservation of energy, i.e., $W_{DC} = W_{AC}$, we have:

$$\Delta W_{DC} = \Delta W_{AC} \tag{3.38}$$

$$\Delta W_{DC} = \Delta(\frac{1}{2}(C_{DC})V_{DC}^2) \tag{3.39}$$

A linearization must be performed to implement the Equation 3.39 which can be derived as:

$$\Delta W_{DC} = C_{DC}V_{DC}\Delta V_{DC} \tag{3.40}$$

In time domain:

$$\Delta W_{DC} = \Delta W_{AC} = \int \Delta P_{AC} dt \tag{3.41}$$

and in frequency domain:

$$\Delta W_{DC} = \frac{\Delta P_{AC}}{s} \tag{3.42}$$

$$C_{DC}V_{DC}\Delta V_{DC} = \frac{\Delta P_{AC}}{s} \tag{3.43}$$

By assuming that $\Delta P'_{AC} = \Delta P'$ and also $\Delta V_{dc} = \begin{bmatrix} \Delta V_{DC} \\ 0 \end{bmatrix}$ we obtain:

$$C_{DC}V_{DC}\Delta V_{DC} = \frac{\Delta P'}{s} \tag{3.44}$$

$$\Delta V_{DC} = \frac{\Delta P'}{C_{DC}V_{DC}s} \tag{3.45}$$

$$\Delta V_{dc} = \begin{bmatrix} \Delta V_{DC} \\ 0 \end{bmatrix} \tag{3.46}$$

$$\Delta V_{dc} = \begin{bmatrix} \frac{1}{C_{DC}V_{DC}s} & 0 \\ 0 & 0 \end{bmatrix} \Delta S \tag{3.47}$$

$$\Delta V_{dc} = DC\Delta S \tag{3.48}$$

By plugging Equation 3.36 into Equation 3.48:

$$\Delta V_{dc} = Kdc\Delta V' + Zdc\Delta I' \tag{3.49}$$

where $Zdc = DC * Io$ and $Kdc = DC * Vo$

3.2.7 Angle Reference Generation

Angle reference is a necessary input for abc/dq and dq/abc blocks in an inverter which can be generated via different methods in different GFM and GFL inverters. Figure 3.1 shows control blocks of different GFM strategies for angle generation. This subsection derives the small-signal model of these angle generation blocks.

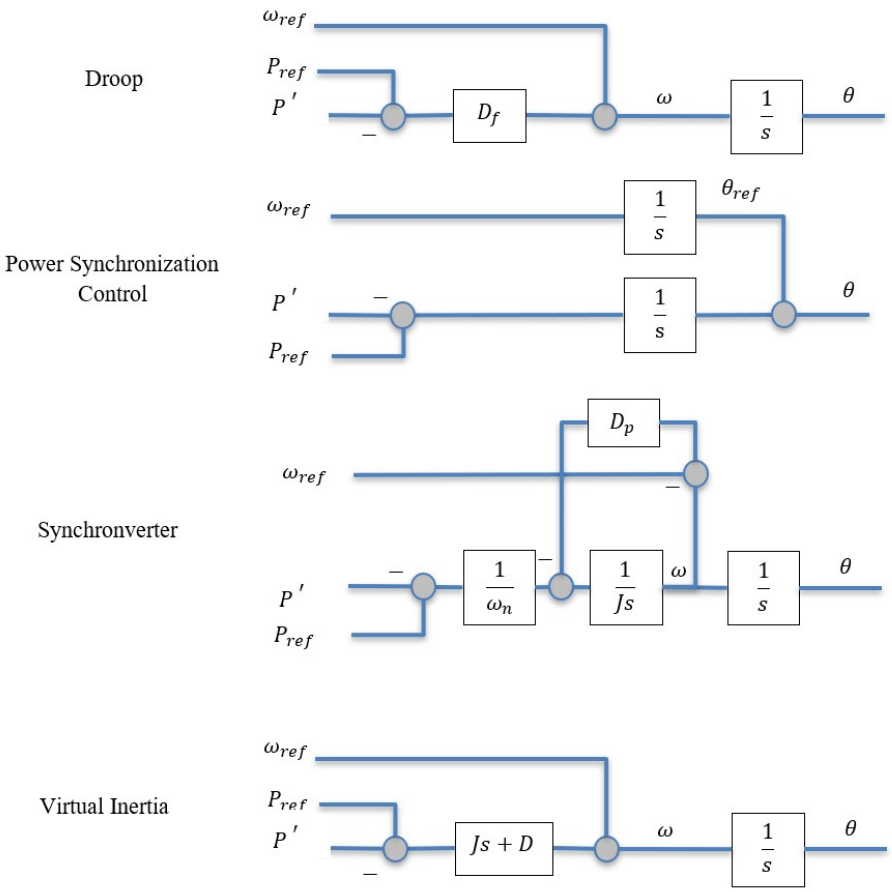

Figure 3.1: GFM strategies for angle generation

GFL-Conventional

In the conventional basic GFL in which $\theta = Constant$, we have:

$$\Delta\theta = 0 \tag{3.50}$$

In order to have a consistant modeling, a new complex variable named $\Delta\theta$ is introduced instead of $\Delta\theta$

$$\Delta T = \begin{bmatrix} 0 \\ \Delta\theta \end{bmatrix} \tag{3.51}$$

Therefore, for the conventional GFL, we have:

$$\Delta T = \begin{bmatrix} 0 \\ 0 \end{bmatrix} \tag{3.52}$$

GFL-PLL

In most of the GFLs, angle reference that is used in dq/abc or abc/dq blocks are generated via PLL. PLL equation is:

$$\Delta\theta = (PI_{pll}/s)\Delta V_q' \tag{3.53}$$

eqs. (3.54) to (3.56) convert PLL equation into ΔT form:

$$\Delta\theta = \begin{bmatrix} (0 & PI_{pll}/s) \end{bmatrix} \Delta V_q' \tag{3.54}$$

$$\Delta T = \begin{bmatrix} 0 & 0 \\ 0 & PI_{pll}s \end{bmatrix} \Delta V' \tag{3.55}$$

$$\Delta T = PLL * \Delta V' \tag{3.56}$$

GFM - Droop Control

Droop control resembles the speed droop property of the governor and trades off deviations of the power injection and frequency deviations from their nominal value [16]:

$$\Delta\theta = \frac{D_f}{s}\Delta P \tag{3.57}$$

$$\Delta T = \begin{bmatrix} 0 & 0 \\ \frac{D_f}{s} & 0 \end{bmatrix} \Delta S \tag{3.58}$$

$$\Delta T = DroopGFM * \Delta S \tag{3.59}$$

GFM - Syn

Synchronvertor (Syn) is a well-known strategy that satisfies the need for a synchronization unit for pre-synchronization purposes, as well as and during normal operation [17].

$$\Delta\theta = \frac{1}{sJ\omega_n(s + \frac{D_p}{J(1+D_pPI_ps)})}\Delta P \tag{3.60}$$

$$\Delta T = \begin{bmatrix} 0 & 0 \\ \frac{1}{sJ\omega_n(s+\frac{D_p}{J(1+D_pPI_ps)})} & 0 \end{bmatrix} \Delta S \tag{3.61}$$

$$\Delta T = SYN * \Delta S \tag{3.62}$$

GFM - Virtual Inertia

The VIL control is a control strategy in which to avoid switching from self-synchronization mode to PLL-mode during grid faults, the use of a PLL is also foreseen during normal operation. Indeed, the output frequency is continuously provided by the PLL, whereas the angle θ is calculated according to a particular equation [17] that can be converted to the small-signal as:

$$\Delta\theta = \frac{1}{Js^2 + Ds}\Delta P \tag{3.63}$$

$$\Delta T = \begin{bmatrix} 0 & 0 \\ \frac{1}{JS^2+Ds} & 0 \end{bmatrix} \Delta S \tag{3.64}$$

$$\Delta T = VIL * \Delta S \tag{3.65}$$

GFM - PSC

The Power Synchronization Control (PSC) is another control strategy where second-order transfer function is implemented in the inner frequency loop, acting on the deviation be-

tween power setpoint and measured power [17].

$$\Delta\theta = \frac{K_i}{s}\Delta P \tag{3.66}$$

$$\Delta T = \begin{bmatrix} 0 & 0 \\ \frac{K_i}{s} & 0 \end{bmatrix} \Delta S \tag{3.67}$$

$$\Delta T = PSC\Delta S \tag{3.68}$$

3.2.8 abc/dq and inverse transform

To properly control the inverter, a abc/dq transfer is necessary. A global dq frame must be considered when considering oscillation between multiple inverters. Both voltage and current signals are converted into a local dq frame to be able to control and then create a global dq frame output. During transients, these two frames may not be exactly the same because of the angle dynamics. In addition, because of the large grid assumption, there is also a steady-state angle difference between both voltage and current global and local dq frames. In this study we will index the local dq frame signals with a prime symbol to distinguish it from the global frame signals.

abc/dq transform:

abc/dq transform in global dq frame is:

$$A' = e^{j\theta}A \tag{3.69}$$

both θ and A values can be perturbed. Therefore, small-signal perturbation of transferred value must consist of both terms. The linear approximation is derived as follows:

$$A' + \Delta A' = e^{j(\theta+\Delta\theta)}(A + \Delta A) \tag{3.70}$$

$$A' + \Delta A' \approx e^{j\theta}(1 + \Delta\theta)(A + \Delta A) \tag{3.71}$$

$$A' + \Delta A' \approx e^{j\theta}(A + \Delta\theta A + \Delta A + \Delta\theta\Delta A) \tag{3.72}$$

By dropping the steady-state and double incremental terms Equation 3.72 will become:

$$\Delta A' \approx e^{j\theta}(A\Delta\theta + \Delta A) \tag{3.73}$$

$$e^{j\theta}A'\Delta\theta = (cos\theta + jsin\theta)(A_d + jA_q)\Delta\theta \tag{3.74}$$

$$e^{j\theta}A'\Delta\theta = ((cos\theta A_d - A_q sin\theta) + j(sin\theta A_d + cos\theta A_d))\Delta\theta \tag{3.75}$$

$$e^{j\theta}A'\Delta\theta = \begin{bmatrix} (cos\theta A_d - A_q sin\theta) \\ (sin\theta A_d + cos\theta A_d) \end{bmatrix} \Delta\theta \tag{3.76}$$

$$\begin{bmatrix} \Delta A'_d \\ \Delta A'_q \end{bmatrix} \approx \begin{bmatrix} (cos\theta A_d - A_q sin\theta) \\ (sin\theta A_d + cos\theta A_d) \end{bmatrix} \Delta\theta + \begin{bmatrix} cos\theta & -sin\theta \\ sin\theta & cos\theta \end{bmatrix} \begin{bmatrix} \Delta A_d \\ \Delta A_q \end{bmatrix} \tag{3.77}$$

considering Equation 3.50, and converting it into matrix, we obtain:

$$\begin{bmatrix} \Delta A'_d \\ \Delta A'_q \end{bmatrix} \approx \begin{bmatrix} 0 & (cos\theta A_d - A_q sin\theta) \\ 0 & (sin\theta A_d + cos\theta A_d) \end{bmatrix} \begin{bmatrix} 0 \\ \Delta\theta \end{bmatrix} + \begin{bmatrix} cos\theta & -sin\theta \\ sin\theta & cos\theta \end{bmatrix} \begin{bmatrix} \Delta A_d \\ \Delta A_q \end{bmatrix} \tag{3.78}$$

$$\Delta A' \approx T_A \Delta T + T_{main} \Delta A \tag{3.79}$$

Finally, the A variable can be replaced with the output voltage and currrent variables:

$$\Delta V_o' = T_V \Delta T + T_{main} \Delta V \tag{3.80}$$

$$\Delta I_o' = T_I \Delta T + T_{main} \Delta I \tag{3.81}$$

$$\Delta V_c' = T_{Vc} \Delta T + T_{main} \Delta V_c \tag{3.82}$$

dq/abc transform:

Similarly in the inverse conversion we have

$$A = e^{-j\theta} A' \tag{3.83}$$

$$A + \Delta A = e^{-j(\theta + \Delta\theta)}(A' + \Delta A') \tag{3.84}$$

$$A + \Delta A \approx e^{-j\theta}(1 - \Delta\theta)(A' + \Delta A') \tag{3.85}$$

$$A + \Delta A \approx e^{-j\theta}(A' - \Delta\theta A' + \Delta A' - \Delta\theta \Delta A') \tag{3.86}$$

By dropping the steady-state and double incremental terms Equation 3.86 will become:

$$\Delta A \approx e^{-j\theta}(\Delta A' - A' \Delta\theta) \tag{3.87}$$

$$e^{-j\theta} A \Delta\theta = (cos\theta - j sin\theta)(A_d' + j A_q')\Delta\theta \tag{3.88}$$

$$e^{-j\theta}A\Delta\theta = ((cos\theta A'_d + A'_q sin\theta) + j(-sin\theta A'_d + cos\theta A'_d))\Delta\theta \tag{3.89}$$

$$e^{j\theta}A\Delta\theta = \begin{bmatrix} (cos\theta A'_d + A'_q sin\theta) \\ (-sin\theta A'_d + cos\theta A'_d) \end{bmatrix} \Delta\theta \tag{3.90}$$

$$\begin{bmatrix} \Delta A_d \\ \Delta A_q \end{bmatrix} \approx \begin{bmatrix} (cos\theta A'_d + A'_q sin\theta) \\ (-sin\theta A'_d + cos\theta A'_d) \end{bmatrix} \Delta\theta + \begin{bmatrix} cos\theta & sin\theta \\ -sin\theta & cos\theta \end{bmatrix} \begin{bmatrix} \Delta A'_d \\ \Delta A'_q \end{bmatrix} \tag{3.91}$$

considering Equation 3.50, matrix conversion of Equation 3.91 will become:

$$\begin{bmatrix} \Delta A_d \\ \Delta A_q \end{bmatrix} \approx \begin{bmatrix} 0 & (cos\theta A'_d + A'_q sin\theta) \\ 0 & (-sin\theta A'_d + cos\theta A'_d) \end{bmatrix} \begin{bmatrix} 0 \\ \Delta\theta \end{bmatrix} + \begin{bmatrix} cos\theta & sin\theta \\ -sin\theta & cos\theta \end{bmatrix} \begin{bmatrix} \Delta A'_d \\ \Delta A'_q \end{bmatrix} \tag{3.92}$$

$$\Delta A \approx T'_A \Delta T + 1/T_{main}\Delta A \tag{3.93}$$

Finally, the actual modulation index formula can be obtained in the matrix form as:

$$\Delta D = T'_D \Delta T + 1/T_{main}\Delta D' \tag{3.94}$$

3.2.9 GFL - Droop

Some GFLs also participate in the voltage and frequency support to the system via GFL droop block which adjusts active and reactive power references based on frequency, and voltage magnitude, respectively. The corresponding equation will be: eqs. (3.95) and (3.96):

$$\Delta P_{ref} = \Delta\theta / m_p \tag{3.95}$$

$$\Delta Q_{ref} = \Delta V_m / n_p \tag{3.96}$$

$$\Delta S_{ref} = \begin{bmatrix} P_{ref} \\ Q_{ref} \end{bmatrix} \tag{3.97}$$

V_m is the output voltage magnitude, which can be written as $V_m = \sqrt{(V_d^2 + V_q^2)}$ and can be linearized as:

$$\Delta V_m = (V_d/V_m)\Delta V_d' + (V_q/V_m)\Delta V_q' \tag{3.98}$$

The prime indices are added to ΔV_m to indicate that it is generated from voltage measurements. $\Delta\theta$ is also calculated in Equation 3.53. Resultant ΔP_{ref} ΔQ_{ref} ΔS_{ref} can be derived as:

$$\Delta P_{ref} = \begin{bmatrix} 0 & PI_{pll}/sm_p \end{bmatrix} \Delta V' \tag{3.99}$$

$$\Delta Q_{ref} = \begin{bmatrix} V_d/V_m n_p & V_q/V_m n_p \end{bmatrix} \Delta V' \tag{3.100}$$

$$\Delta S_{ref} = \begin{bmatrix} 0 & PI_{pll}/sm_p \\ V_d/V_m n_p & V_q/V_m n_p \end{bmatrix} \Delta V' \tag{3.101}$$

$$\Delta S_{ref} = DroopGFL\Delta V' \tag{3.102}$$

3.3 Section Summary

Figure 3.2 summarizes block diagram representation of both GFM and GFL inverter complex models. In Figure 3.2 each signal is a 2×1 matrix (for example $\begin{bmatrix} \Delta V_d \\ \Delta V_q \end{bmatrix}$ $\begin{bmatrix} \Delta I_d \\ \Delta I_q \end{bmatrix}$ $\begin{bmatrix} \Delta P \\ \Delta Q \end{bmatrix}$ and $\begin{bmatrix} \Delta\theta \\ 0 \end{bmatrix}$) and each transfer block is a 2×2 matrix of transfer functions, $\begin{bmatrix} Xdd & Xdq \\ Xqd & Xqq \end{bmatrix}$ or a linear function of two 2×2 matrices when there are two inputs ($A \begin{bmatrix} Xdd & Xdq \\ Xqd & Xqq \end{bmatrix} +$

$B \begin{bmatrix} Ydd & Ydq \\ Yqd & Yqq \end{bmatrix}$). In Figure 3.2, the red parts are only for GFL converters, and blue characters are only for GFM converters. The linearized block diagrams are shown in Figure 3.3.

As shown in the Figure 3.2, the small-signal model of the GFL converter is built considering the abc/dq effect. Under voltage disturbance, this block generates an error between the converter and global dq frames. The effect of ΔT on the measured small-signal currents and voltages in both GFL and GFM topology is shown. The noticeable point in Figure 3.2 is how the generation of ΔT is different in GFL and GFM. The figure shows that the GFM ΔT is generated using both ΔI and ΔV signals, whereas the GFL ΔT is only made from ΔV. Therefore, complexity doubles in the GFM, and more poles will be added to the final small-signal impedance.

The difference between GFM and GFL is the existence of ΔI alongside ΔV in reference angle generation. The way that this extra term affects the number of poles will be further discussed in subsection 5.1.1.

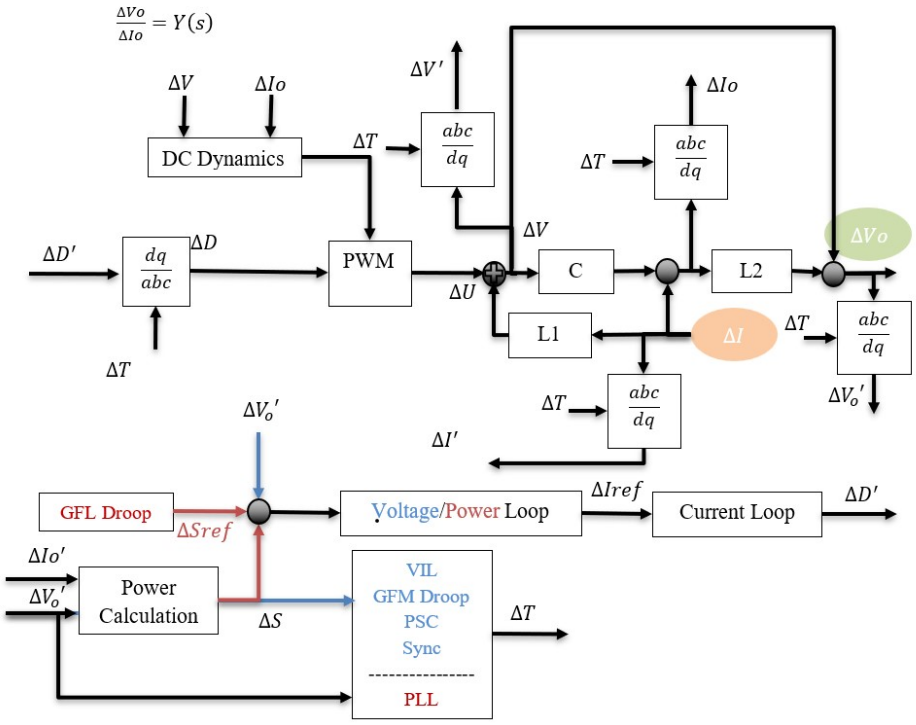

Figure 3.2: Exact Inverter small-signal model in matrix form. Black lines and text are for both GFM and GFL, blue lines and text are only for GFM, and red lines and text are only for GFL.

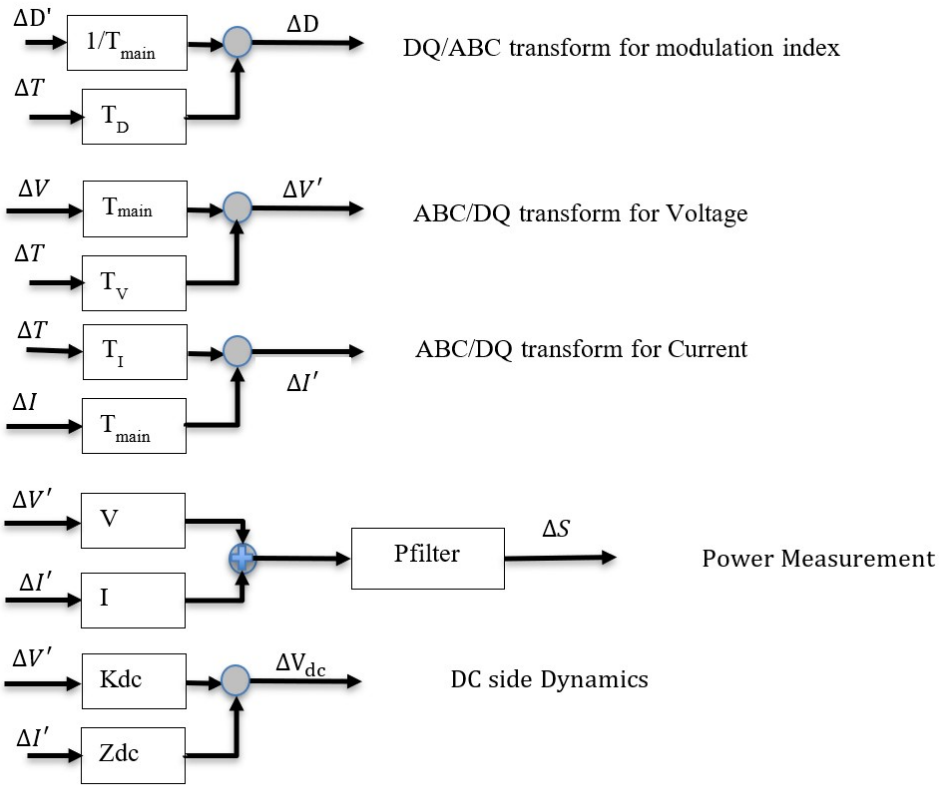

Figure 3.3: Linearized block diagrams of the inverters.

CHAPTER 4
COMPUTATIONAL IMPLEMENTATION

A computational method for inverter impedance calculation is introduced and implemented in this study and presented in this chapter. The computational approach is chosen to handle the sizeable parametric matrix calculations and prevent human error during model calculations. First, the computational procedure is explained, and later, the resultant models are presented for each inverter of subsection 3.2.7.

4.1 Computational Procedure

In section 3.2 all block equations are finally converted into matrix form with 2×2 parameters and 1×2 variables. With this kind of mapping, without loss of generality, all the blocks can be put into a set of algebraic equations of scalar parameters and scalar variables and can be solved via scalar equation solvers. The results of this derivation are presented in section 4.2. Because these results can be saved once and used later rather than solving the equation each time, this approach is computationally efficient. After saving the results, the variables will be eliminated, and 2×2 parameters are plugged to result into a final admittance/impedance 2×2 parameter. After this calculation, the results of each component, dd, dq, qd, and qq, for each inverter are saved separately, preferably as a character data class in the computer. Finally, the latter formulas can be used for each instance of parameters to derive the numerical transfer functions.

4.2 Small Signal Impedance Results

The algebraic solution of matrix equation for each inverter is presented here:

For the GFM inverters the nominators and denominators are presented separately due

to their complexity.

Grid Following Inverter: Conventional Model

$$Z_{GFL} = \frac{\begin{array}{r} Z_{L1} - Z_{L2} - Deld * Kdc - Delv * L1w \\ +Delv * PIC + Delv * FV * Z_{L2} + Deld * Ydc * Z_{L2} \\ +Z_c * Z_{L1} * Z_{L2} + Delv * PIC * PIS * V - Delv * L1w * Z_c * Z_{L2} \\ +Delv * PIC * Z_c * Z_{L2} - Delv * I * PIC * PIS * Z_{L2} \end{array}}{\begin{array}{r} Z_c * Z_{L1} + Delv * FV + Deld * Ydc \\ -Delv * L1w * Z_c + Delv * PIC * Z_c - Delv * I * PIC * PIS - 1 \end{array}} \quad (4.1)$$

Grid Following Inverter: Exact Model

$$Z_{GFL-Exact} = \frac{\begin{array}{r} Z_{L1} - Z_{L2} - Delv * L1w + Delv * PIC \\ +Delv * FV * Z_{L2} - PLL * Tv * Z_{L1} + \\ PLL * Tv * Z_{L2} + Z_c * Z_{L1} * Z_{L2} + Delv * L1w * PLL * Tv - \\ Delv * PIC * PLL * Tv - Delv * L1w * Z_c * Z_{L2} + \\ Delv * PIC * Z_c * Z_{L2} - PLL * Tv * Z_c * Z_{L1} * Z_{L2} + \\ Delv * Droop * PIC * PIS * Z_{L2} + Delv * PFilter * PIC * PIS * V + \\ Delv * L1w * PLL * Ti * Z_{L2} - Delv * PIC * PLL * Ti * Z_{L2} \\ +Delv * PLL * Td * Tmain * Z_{L2} - Delv * I * PFilter * PIC * PIS * Z_{L2} \\ +Delv * L1w * PLL * Tv * Z_c * Z_{L2} \\ -Delv * PIC * PLL * Tv * Z_c * Z_{L2} \\ -Delv * PFilter * PIC * PIS * PLL * Tv * V \\ -Delv * PFilter * PIC * PIS * PLL * Tio * V * Z_{L2} \end{array}}{\begin{array}{r} PLL * Tv + Z_c * Z_{L1} + Delv * FV \\ -Delv * L1w * Z_c + Delv * PIC * Z_c \\ +Delv * Droop * PIC * PIS \\ +Delv * L1w * PLL * Ti - Delv * PIC * PLL * Ti + \\ Delv * PLL * Td * Tmain \\ -PLL * Tv * Z_c * Z_{L1} - \\ Delv * I * PFilter * PIC * PIS + Delv * L1w * PLL * Tv * Z_c - \\ Delv * PIC * PLL * Tv * Z_c \\ -Delv * PFilter * PIC * PIS * PLL * Tio * V - 1 \end{array}} \tag{4.2}$$

$$\mathbf{Z}_{GFM-droop}(Nominator) = Z_{L1} - Z_{L2} - Delv * L1w + Delv * PIC - Cw * Delv * PIC - Delv * FII * PIC + Delv * FV * Z_{L2} + Z_c * Z_{L1} * Z_{L2} - Delv * PIC * PIV * Z_{L2} - Delv * L1w * Z_c * Z_{L2} + Delv * PIC * Z_c * Z_{L2} - Cw * Delv * PIC * Z_c * Z_{L2} - DroopGFM * I * PFilter * Tv * Z_{L1} + DroopGFM * I * PFilter * Tv * Z_{L2} - Delv * FII * PIC * Z_c * Z_{L2} - DroopGFM * PFilter * Tio * V * Z_{L1} + DroopGFM * PFilter * Tio * V * Z_{L2} + Delv * DroopGFM * I * L1w * PFilter * Tv - Delv * DroopGFM * I * PFilter * PIC * Tv - Delv * DroopGFM * FV * PFilter * Tv * V - Delv * DroopGFM * L1w * PFilter * Ti * V + Delv * DroopGFM * L1w * PFilter * Tio * V + Delv * DroopGFM * PFilter * PIC * Ti * V - Delv * DroopGFM * PFilter * PIC * Tio * V - Delv * DroopGFM * PFilter * Td * Tmain * V + Cw * Delv * DroopGFM * I * PFilter * PIC * Tv + Delv * DroopGFM * FII * I * PFilter * PIC * Tv - Cw * Delv * DroopGFM * PFilter * PIC * Ti * V + Cw * Delv * DroopGFM * PFilter * PIC * Tio * V - Delv * DroopGFM * FII * PFilter * PIC * Ti * V + Delv * DroopGFM * FII * PFilter * PIC * Tio * V + Delv * DroopGFM * I * L1w * PFilter * Ti * Z_{L2} - Delv * DroopGFM * I * PFilter * PIC * Ti * Z_{L2} + Delv * DroopGFM * PFilter * PIC * PIV * Tv * V - Delv * DroopGFM * FV * PFilter * Tio * V * Z_{L2} + Delv * DroopGFM * I * PFilter * Td * Tmain * Z_{L2} - DroopGFM * I * PFilter * Tv * Z_c * Z_{L1} * Z_{L2} - DroopGFM * PFilter * Tio * V * Z_c * Z_{L1} * Z_{L2} + Cw * Delv * DroopGFM * I * PFilter * PIC * Ti * Z_{L2} + Delv * DroopGFM * FII * I * PFilter * PIC * Ti * Z_{L2} + Delv * DroopGFM * I * L1w * PFilter * Tv * Z_c * Z_{L2} - Delv * DroopGFM * I * PFilter * PIC * Tv * Z_c * Z_{L2} + Delv * DroopGFM * PFilter * PIC * PIV * Tio * V * Z_{L2} + Delv * DroopGFM * L1w * PFilter * Tio * V * Z_c * Z_{L2} - Delv * DroopGFM * PFilter * PIC * Tio * V * Z_c * Z_{L2} + Cw * Delv * DroopGFM * I * PFilter * PIC * Tv * Z_c * Z_{L2} + Delv * DroopGFM * FII * I * PFilter * PIC * Tv * Z_c * Z_{L2} + Cw * Delv * DroopGFM * PFilter * PIC * Tio * V * Z_c * Z_{L2} + Delv * DroopGFM * FII * PFilter * PIC * Tio * V * Z_c * Z_{L2}$$

(4.3)

$$\mathbf{Z}_{GFM-droop}(Denominator) = Z_c*Z_{L1}+Delv*FV-Delv*PIC*PIV-Delv*L1w*Z_c+Delv*PIC*Z_c-Cw*Delv*PIC*Z_c+DroopGFM*I*PFilter*Tv-Delv*FII*PIC*Z_c+DroopGFM*PFilter*Tio*V+Delv*DroopGFM*I*L1w*PFilter*Ti-Delv*DroopGFM*I*PFilter*PIC*Ti-Delv*DroopGFM*FV*PFilter*Tio*V+Delv*DroopGFM*I*PFilter*Td*Tmain-DroopGFM*I*PFilter*Tv*Z_c*Z_{L1}-DroopGFM*PFilter*Tio*V*Z_c*Z_{L1}+Cw*Delv*DroopGFM*I*PFilter*PIC*Ti+Delv*DroopGFM*FII*I*PFilter*PIC*Ti+Delv*DroopGFM*I*L1w*PFilter*Tv*Z_c-Delv*DroopGFM*I*PFilter*PIC*Tv*Z_c+Delv*DroopGFM*PFilter*PIC*PIV*Tio*V+Delv*DroopGFM*L1w*PFilter*Tio*V*Z_c-Delv*DroopGFM*PFilter*PIC*Tio*V*Z_c+Cw*Delv*DroopGFM*I*PFilter*PIC*Tv*Z_c+Delv*DroopGFM*FII*I*PFilter*PIC*Tv*Z_c+Cw*Delv*DroopGFM*PFilter*PIC*Tio*V*Z_c+Delv*DroopGFM*FII*PFilter*PIC*Tio*V*Z_c-1$$

(4.4)

$$\mathbf{Z}_{GFM-PSC}(Nominator) = Z_{L1} - Z_{L2} - Delv*L1w + Delv*PIC - Cw*Delv*PIC - Delv*FII*PIC + Delv*FV*Z_{L2} + Z_c*Z_{L1}*Z_{L2} - Delv*PIC*PIV*Z_{L2} - Delv*L1w*Z_c*Z_{L2} + Delv*PIC*Z_c*Z_{L2} - PFilter*PSC*Tio*V*Z_{L1} + PFilter*PSC*Tio*V*Z_{L2} - Cw*Delv*PIC*Z_c*Z_{L2} - Delv*FII*PIC*Z_c*Z_{L2} - I*PFilter*PSC*Tv*Z_{L1} + I*PFilter*PSC*Tv*Z_{L2} + Delv*I*L1w*PFilter*PSC*Tv - Delv*I*PFilter*PIC*PSC*Tv - Delv*FV*PFilter*PSC*Tv*V - Delv*L1w*PFilter*PSC*Ti*V + Delv*L1w*PFilter*PSC*Tio*V + Delv*PFilter*PIC*PSC*Ti*V - Delv*PFilter*PIC*PSC*Tio*V - Delv*PFilter*PSC*Td*Tmain*V + Cw*Delv*I*PFilter*PIC*PSC*Tv + Delv*FII*I*PFilter*PIC*PSC*Tv - Cw*Delv*PFilter*PIC*PSC*Ti*V + Cw*Delv*PFilter*PIC*PSC*Tio*V - Delv*FII*PFilter*PIC*PSC*Ti*V + Delv*FII*PFilter*PIC*PSC*Tio*V + Delv*I*L1w*PFilter*PSC*Ti*Z_{L2} - Delv*I*PFilter*PIC*PSC*Ti*Z_{L2} + Delv*PFilter*PIC*PIV*PSC*Tv*V - Delv*FV*PFilter*PSC*Tio*V*Z_{L2} + Delv*I*PFilter*PSC*Td*Tmain*Z_{L2} - I*PFilter*PSC*Tv*Z_c*Z_{L1}*Z_{L2} - PFilter*PSC*Tio*V*Z_c*Z_{L1}*Z_{L2} + Cw*Delv*I*PFilter*PIC*PSC*Ti*Z_{L2} + Delv*FII*I*PFilter*PIC*PSC*Ti*Z_{L2} + Delv*I*L1w*PFilter*PSC*Tv*Z_c*Z_{L2} - Delv*I*PFilter*PIC*PSC*Tv*Z_c*Z_{L2} + Delv*PFilter*PIC*PIV*PSC*Tio*V*Z_{L2} + Delv*L1w*PFilter*PSC*Tio*V*Z_c*Z_{L2} - Delv*PFilter*PIC*PSC*Tio*V*Z_c*Z_{L2} + Cw*Delv*I*PFilter*PIC*PSC*Tv*Z_c*Z_{L2} + Delv*FII*I*PFilter*PIC*PSC*Tv*Z_c*Z_{L2} + Cw*Delv*PFilter*PIC*PSC*Tio*V*Z_c*Z_{L2} + Delv*FII*PFilter*PIC*PSC*Tio*V*Z_c*Z_{L2} \quad (4.5)$$

$$\mathbf{Z}_{GFM-PSC}(Denominator) = Z_c * Z_{L1} + Delv * FV - Delv * PIC * PIV - Delv * L1w * Z_c + Delv * PIC * Z_c - Cw * Delv * PIC * Z_c - Delv * FII * PIC * Z_c + I * PFilter * PSC * Tv + PFilter * PSC * Tio * V + Delv * I * L1w * PFilter * PSC * Ti - Delv * I * PFilter * PIC * PSC * Ti - Delv * FV * PFilter * PSC * Tio * V + Delv * I * PFilter * PSC * Td * Tmain - I * PFilter * PSC * Tv * Z_c * Z_{L1} - PFilter * PSC * Tio * V * Z_c * Z_{L1} + Cw * Delv * I * PFilter * PIC * PSC * Ti + Delv * FII * I * PFilter * PIC * PSC * Ti + Delv * I * L1w * PFilter * PSC * Tv * Z_c - Delv * I * PFilter * PIC * PSC * Tv * Z_c + Delv * PFilter * PIC * PIV * PSC * Tio * V + Delv * L1w * PFilter * PSC * Tio * V * Z_c - Delv * PFilter * PIC * PSC * Tio * V * Z_c + Cw * Delv * I * PFilter * PIC * PSC * Tv * Z_c + Delv * FII * I * PFilter * PIC * PSC * Tv * Z_c + Cw * Delv * PFilter * PIC * PSC * Tio * V * Z_c + Delv * FII * PFilter * PIC * PSC * Tio * V * Z_c - 1 \quad (4.6)$$

Grid Forming Inverter: Synchronvector

$$\mathbf{Z}_{GFM-SYN}(Nominator) = Z_{L1} - Z_{L2} - Delv*L1w + Delv*PIC - Cw*Delv*PIC - Delv*FII*PIC + Delv*FV*Z_{L2} + Z_c*Z_{L1}*Z_{L2} - Delv*PIC*PIV*Z_{L2} - Delv*L1w*Z_c*Z_{L2} + Delv*PIC*Z_c*Z_{L2} - PFilter*SYN*Tio*V*Z_{L1} + PFilter*SYN*Tio*V*Z_{L2} - Cw*Delv*PIC*Z_c*Z_{L2} - Delv*FII*PIC*Z_c*Z_{L2} - I*PFilter*SYN*Tv*Z_{L1} + I*PFilter*SYN*Tv*Z_{L2} + Delv*I*L1w*PFilter*SYN*Tv - Delv*I*PFilter*PIC*SYN*Tv - Delv*FV*PFilter*SYN*Tv*V - Delv*L1w*PFilter*SYN*Ti*V + Delv*L1w*PFilter*SYN*Tio*V + Delv*PFilter*PIC*SYN*Ti*V - Delv*PFilter*PIC*SYN*Tio*V - Delv*PFilter*SYN*Td*Tmain*V + Cw*Delv*I*PFilter*PIC*SYN*Tv + Delv*FII*I*PFilter*PIC*SYN*Tv - Cw*Delv*PFilter*PIC*SYN*Ti*V + Cw*Delv*PFilter*PIC*SYN*Tio*V - Delv*FII*PFilter*PIC*SYN*Ti*V + Delv*FII*PFilter*PIC*SYN*Tio*V + Delv*I*L1w*PFilter*SYN*Ti*Z_{L2} - Delv*I*PFilter*PIC*SYN*Ti*Z_{L2} + Delv*PFilter*PIC*PIV*SYN*Tv*V - Delv*FV*PFilter*SYN*Tio*V*Z_{L2} + Delv*I*PFilter*SYN*Td*Tmain*Z_{L2} - I*PFilter*SYN*Tv*Z_c*Z_{L1}*Z_{L2} - PFilter*SYN*Tio*V*Z_c*Z_{L1}*Z_{L2} + Cw*Delv*I*PFilter*PIC*SYN*Ti*Z_{L2} + Delv*FII*I*PFilter*PIC*SYN*Ti*Z_{L2} + Delv*I*L1w*PFilter*SYN*Tv*Z_c*Z_{L2} - Delv*I*PFilter*PIC*SYN*Tv*Z_c*Z_{L2} + Delv*PFilter*PIC*PIV*SYN*Tio*V*Z_{L2} + Delv*L1w*PFilter*SYN*Tio*V*Z_c*Z_{L2} - Delv*PFilter*PIC*SYN*Tio*V*Z_c*Z_{L2} + Cw*Delv*I*PFilter*PIC*SYN*Tv*Z_c*Z_{L2} + Delv*FII*I*PFilter*PIC*SYN*Tv*Z_c*Z_{L2} + Cw*Delv*PFilter*PIC*SYN*Tio*V*Z_c*Z_{L2} + Delv*FII*PFilter*PIC*SYN*Tio*V*Z_c*Z_{L2} \quad (4.7)$$

$$\mathbf{Z}_{GFM-SYN}(Denominator) = Z_c * Z_{L1} + Delv * FV - Delv * PIC * PIV - Delv * L1w * Z_c + Delv * PIC * Z_c - Cw * Delv * PIC * Z_c - Delv * FII * PIC * Z_c + I * PFilter * SYN * Tv + PFilter * SYN * Tio * V + Delv * I * L1w * PFilter * SYN * Ti - Delv * I * PFilter * PIC * SYN * Ti - Delv * FV * PFilter * SYN * Tio * V + Delv * I * PFilter * SYN * Td * Tmain - I * PFilter * SYN * Tv * Z_c * Z_{L1} - PFilter * SYN * Tio * V * Z_c * Z_{L1} + Cw * Delv * I * PFilter * PIC * SYN * Ti + Delv * FII * I * PFilter * PIC * SYN * Ti + Delv * I * L1w * PFilter * SYN * Tv * Z_c - Delv * I * PFilter * PIC * SYN * Tv * Z_c + Delv * PFilter * PIC * PIV * SYN * Tio * V + Delv * L1w * PFilter * SYN * Tio * V * Z_c - Delv * PFilter * PIC * SYN * Tio * V * Z_c + Cw * Delv * I * PFilter * PIC * SYN * Tv * Z_c + Delv * FII * I * PFilter * PIC * SYN * Tv * Z_c + Cw * Delv * PFilter * PIC * SYN * Tio * V * Z_c + Delv * FII * PFilter * PIC * SYN * Tio * V * Z_c - 1 \quad (4.8)$$

$$\mathbf{Z}_{GFM-VIL}(Nominator) = Z_{L1} - Z_{L2} - Delv * L1w + Delv * PIC - Cw * Delv * PIC - Delv * FII * PIC + Delv * FV * Z_{L2} + Z_c * Z_{L1} * Z_{L2} - Delv * PIC * PIV * Z_{L2} - Delv * L1w * Z_c * Z_{L2} + Delv * PIC * Z_c * Z_{L2} - PFilter * Tio * V * VIL * Z_{L1} + PFilter * Tio * V * VIL * Z_{L2} - Cw * Delv * PIC * Z_c * Z_{L2} - Delv * FII * PIC * Z_c * Z_{L2} - I * PFilter * Tv * VIL * Z_{L1} + I * PFilter * Tv * VIL * Z_{L2} + Delv * I * L1w * PFilter * Tv * VIL - Delv * I * PFilter * PIC * Tv * VIL - Delv * FV * PFilter * Tv * V * VIL - Delv * L1w * PFilter * Ti * V * VIL + Delv * L1w * PFilter * Tio * V * VIL + Delv * PFilter * PIC * Ti * V * VIL - Delv * PFilter * PIC * Tio * V * VIL - Delv * PFilter * Td * Tmain * V * VIL + Cw * Delv * I * PFilter * PIC * Tv * VIL + Delv * FII * I * PFilter * PIC * Tv * VIL - Cw * Delv * PFilter * PIC * Ti * V * VIL + Cw * Delv * PFilter * PIC * Tio * V * VIL - Delv * FII * PFilter * PIC * Ti * V * VIL + Delv * FII * PFilter * PIC * Tio * V * VIL + Delv * I * L1w * PFilter * Ti * VIL * Z_{L2} - Delv * I * PFilter * PIC * Ti * VIL * Z_{L2} + Delv * PFilter * PIC * PIV * Tv * V * VIL - Delv * FV * PFilter * Tio * V * VIL * Z_{L2} + Delv * I * PFilter * Td * Tmain * VIL * Z_{L2} - I * PFilter * Tv * VIL * Z_c * Z_{L1} * Z_{L2} - PFilter * Tio * V * VIL * Z_c * Z_{L1} * Z_{L2} + Cw * Delv * I * PFilter * PIC * Ti * VIL * Z_{L2} + Delv * FII * I * PFilter * PIC * Ti * VIL * Z_{L2} + Delv * I * L1w * PFilter * Tv * VIL * Z_c * Z_{L2} - Delv * I * PFilter * PIC * Tv * VIL * Z_c * Z_{L2} + Delv * PFilter * PIC * PIV * Tio * V * VIL * Z_{L2} + Delv * L1w * PFilter * Tio * V * VIL * Z_c * Z_{L2} - Delv * PFilter * PIC * Tio * V * VIL * Z_c * Z_{L2} + Cw * Delv * I * PFilter * PIC * Tv * VIL * Z_c * Z_{L2} + Delv * FII * I * PFilter * PIC * Tv * VIL * Z_c * Z_{L2} + Cw * Delv * PFilter * PIC * Tio * V * VIL * Z_c * Z_{L2} + Delv * FII * PFilter * PIC * Tio * V * VIL * Z_c * Z_{L2} \tag{4.9}$$

$$\mathbf{Z}_{GFM-VIL}(Denominator) = Z_c * Z_{L1} + Delv * FV - Delv * PIC * PIV - Delv * L1w * Z_c + Delv * PIC * Z_c - Cw * Delv * PIC * Z_c - Delv * FII * PIC * Z_c + I * PFilter * Tv * VIL + PFilter * Tio * V * VIL + Delv * I * L1w * PFilter * Ti * VIL - Delv * I * PFilter * PIC * Ti * VIL - Delv * FV * PFilter * Tio * V * VIL + Delv * I * PFilter * Td * Tmain * VIL - I * PFilter * Tv * VIL * Z_c * Z_{L1} - PFilter * Tio * V * VIL * Z_c * Z_{L1} + Cw * Delv * I * PFilter * PIC * Ti * VIL + Delv * FII * I * PFilter * PIC * Ti * VIL + Delv * I * L1w * PFilter * Tv * VIL * Z_c - Delv * I * PFilter * PIC * Tv * VIL * Z_c + Delv * PFilter * PIC * PIV * Tio * V * VIL + Delv * L1w * PFilter * Tio * V * VIL * Z_c - Delv * PFilter * PIC * Tio * V * VIL * Z_c + Cw * Delv * I * PFilter * PIC * Tv * VIL * Z_c + Delv * FII * I * PFilter * PIC * Tv * VIL * Z_c + Cw * Delv * PFilter * PIC * Tio * V * VIL * Z_c + Delv * FII * PFilter * PIC * Tio * V * VIL * Z_c - 1 \quad (4.10)$$

4.3 Matrix Substitution

In the next step, each term of the above equations is replaced with its corresponding complex matrix. A list of All Terms with their Complex form is presented in tables 4.1 and 4.2.

4.4 Parameters Substitution and Tuning

After matrix substitution, Four parametric transfer functions will be generated for each of the inverters of subsection 3.2.7. Some of these parameters, such as system frequency ω are determined by the system. Whereas, semiconductor, LCL, and DC elements (L_1, L_2, C, and C_{DC} and T_{del}), are determined via inverter hardware design process. In addition, voltage magnitude and angle reference, which are not dependent on each other ($tan\theta = V_q/V_d$)

Table 4.1: Matrix Arrays of Parameters

Parameter	dd	dq	qd	qq
Vo	V_{do}	V_{qo}	V_{qo}	-V_{do}
Io	I_{do}	I_{qo}	-I_{qo}	I_{do}
Z_{L1}	sL_1	-ωL_1	ωL_1	sL_1
L1w	0	-ωL_1	ωL_1	0
Z_{L2}	sL_2	-ωL_2	ωL_2	sL_2
L2w	0	-ωL_1	ωL_1	0
Z_c	sC	-ωC	ωC	sC
Cw	0	-ωC	ωC	0
PIC	$KP_c + KI_c/s$	0	0	$KP_c + KI_c/s$
Fv	$K_{vf}/(1 + T_{vf}s)$	0	0	$K_{vf}/(1 + T_{vf}s)$
FII	$K_{vii}/(1 + T_{vii}s)$	0	0	$K_{vii}/(1 + T_{vii}s)$
PIS	$KP_p + KI_p/s$	0	0	$KP_q + KI_q/s$
PIV	$KP_pV + KI_pV/s$	0	0	$KP_qV + KI_qV/s$
PFilter	$\omega_c/s + \omega_c$	0	0	$\omega_c/s + \omega_c$
PLL	0	0	0	$KP_{pll} + KI_{pll}/s$
Droop	0	$KP_{pll} + KI_{pll}/s$	$V_d/n\sqrt{V_d^2 + V_q^2}$	$V_q/n\sqrt{V_d^2 + V_q^2}$

Table 4.2: Matrix Arrays of Parameters

Parameter	dd	dq	qd	qq
DroopGFL	D_f/s	D_f/s	0	0
VIL	$1/(Js^2 + D_{vil}s)$	$1/(Js^2 + D_{vil}s)$	0	0
SYN	$\frac{1}{sJ\omega_n(s+\frac{D_p}{J(1+D_pPI_ps)})}$	$\frac{1}{sJ\omega_n(s+\frac{D_p}{J(1+D_pPI_ps)})}$	0	0
PSC	K_pSC/s	K_pSC/s	0	0
K_{DC}	$I_d/C_{DC}V_{DC}$	$I_q/C_{DC}V_{DC}$	0	0
Y_{DC}	$V_d/C_{DC}V_{DC}$	$V_q/C_{DC}V_{DC}$	0	0
DelD	$D(\frac{1-0.5T_{del}s}{1+0.5T_{del}s})$	0	0	$D(\frac{1-0.5T_{del}s}{1+0.5T_{del}s})$
Delv	$Vdc(\frac{1-0.5T_{del}s}{1+0.5T_{del}s})$	0	0	$Vdc(\frac{1-0.5T_{del}s}{1+0.5T_{del}s})$
TETA	$cos(\theta)$	$sin(\theta)$	$-sin(\theta)$	$cos(\theta)$
T_v	0	$-sin(\theta)V_d + cos(\theta)V_q$	0	$-cos(\theta)I_d - sin(\theta)I_q$
T_{io}	0	$-sin(\theta)Io_d + cos(\theta)Io_q$	0	$-cos(\theta)Io_d - sin(\theta)Io_q$
T_i	0	$-sin(\theta)I_d + cos(\theta)I_q$	0	$-cos(\theta)I_d - sin(\theta)I_q$
T_d	0	$cos(\theta)D_d + sin(\theta)D_q$	0	$-sin(\theta)D_d + cos(\theta)D_q$

and also GFM droop control coefficients are determined via grid operation. Finally, the rest of the coefficients are implemented locally on a control board. In this design hierarchy, the goal is to achieve the best performance with the given parameters of an upper-level study. However, upper-level adjustments are required if the goal cannot be achieved. Although there are systematic methods such as [18] to search for the best parameters, they are limited to a particular type of inverter and also are designed for a more limited inverter model. In the chapter 5 an approach has been made to tune these parameters. Figure 4.1 summarizes the parameters of small-signal modeling and their corresponding study.

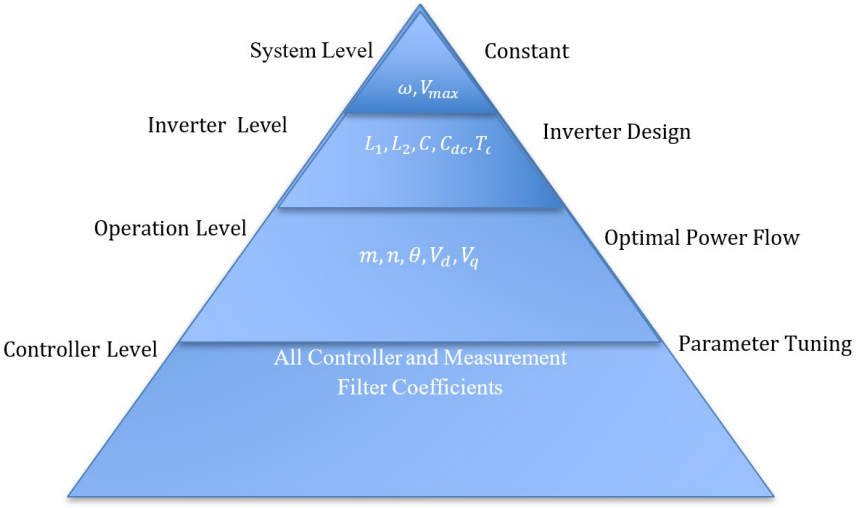

Figure 4.1: Hierarchy of Small Signal Derivation

CHAPTER 5

RESULTS AND DISCUSSION

5.1 Inverter Type Small Signal Comparison of GFMs

In this section, the inverter control strategies mentioned in chapters 3 and 4 are compared in terms of eigenvalues, time domains, and frequency domain.

5.1.1 Eigenvalue Analysis

Table 5.1: Number of Eigenvalues for Each Strategy

Inverter Strategy	GFL basic	GFL	GFM_{PSC}	GFM_{droop}	GFM_{syn}	GFM_{VIL}
Number of dd poles	12	12	17	17	21	16
Number of dq poles	17	17	16	16	20	16
Number of qd poles	19	19	13	13	17	19
Number of qq poles	13	17	15	15	19	20

The number of poles or equivalently eigenvalues in different inverter control strategies are shown in Table 5.1. Results in Table 5.1 show that the GFM has the most complexity in terms of eigenvalues, and GFL_{basic} which is a conventional GFL model, has the minimum number of poles. Another note-worthy point is that the number of poles is inconsistently different in control strategies, and usually, they have different matrix elements with maximum complexity.

5.1.2 Frequency Domain Analysis

In this subsection the optimal response of the inverters are reported using Bode diagrams. The optimal parameters are derived via comprehensive trials and errors with consideration of parameter dependencies in power flow and also complying with the cascaded controller design strategy obtained from [18].

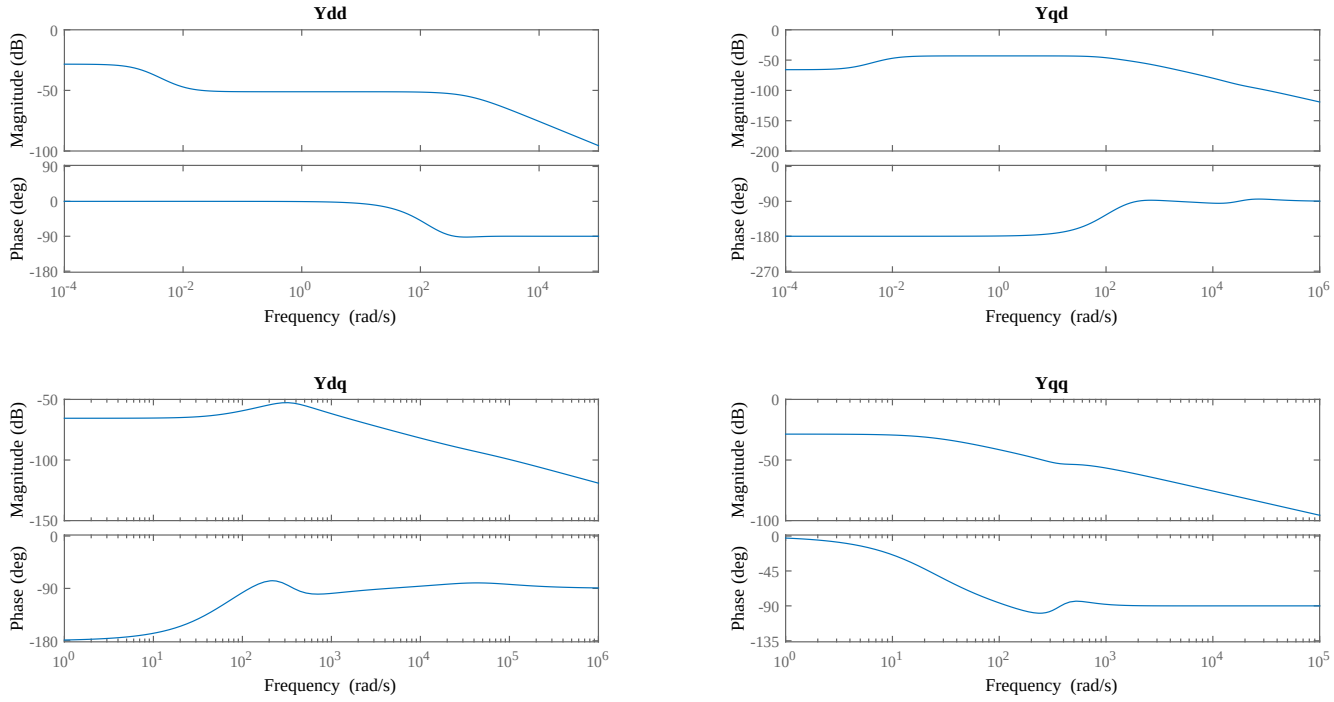

Figure 5.1: Bode diagram of droop inverter with optimal parameters

Figure 5.1 represents the bode response of the Droop GFM. The results show that all the gains are negative, meaning that with the optimal parameters, any disturbance with any frequency will have a lower magnitude and be damped. In addition, all Y_{dd}, Y_{qd}, Y_{dq}, and Y_{qq} are acting as a low-pass filter meaning that no high-frequency oscillation will affect the inverter performance.

Figure 5.2 shows the bode diagram of VIL inverter. It can be seen that due to the additional term in ΔT generation, a new pole with the frequency of nearly 10^2 rad/s is added, which makes the response more complex than the Droop. It also means that for any oscillation in the system, a transient with the frequency of 10^2 rad/s will circulate in the system. This specific pole will increase the gain in Y_{qd} and Y_{dd} to more than 0 dB if an oscillation near 10^2 (rad/s) happens.

Figure 5.3 shows the bode results the PSC inverter. The results show a stable behavior in Ydq and Yqd. However, in the vicinity of a specific pole, the magnitude becomes more

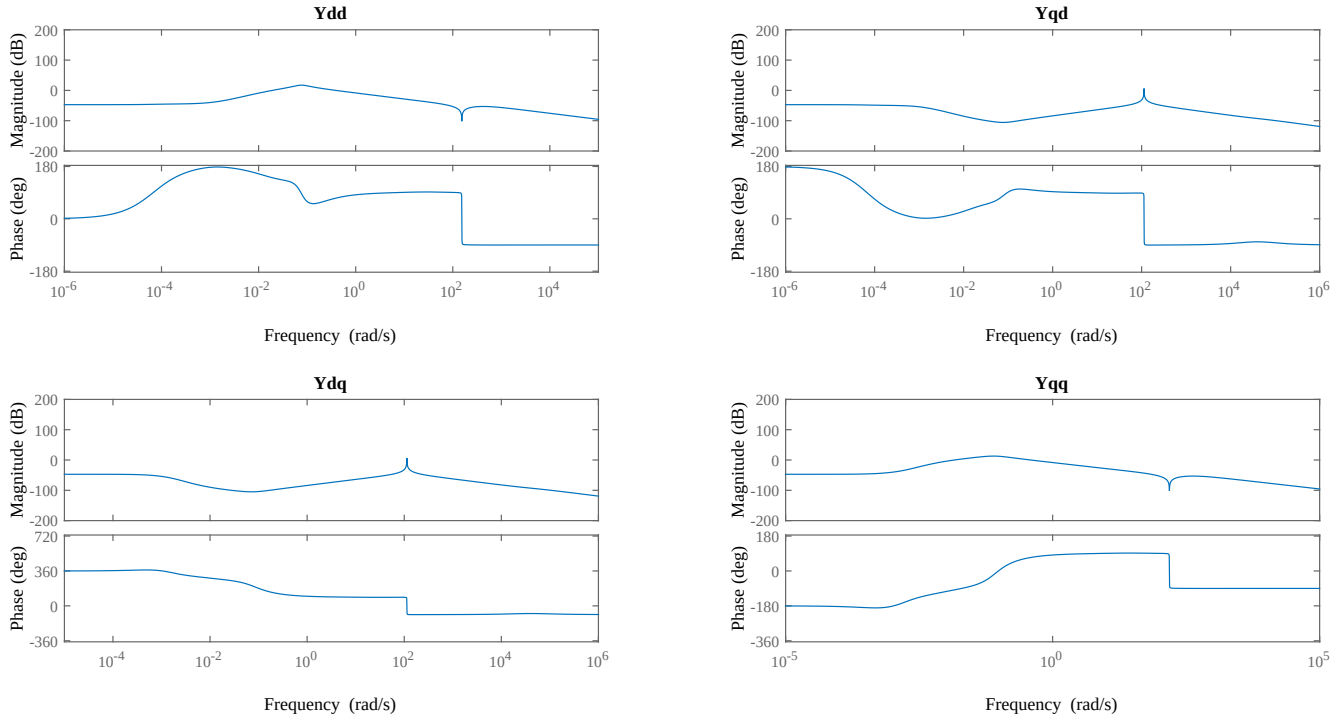

Figure 5.2: Bode diagram of VIL inverter with optimal parameters

than $0(dB)$. Another Noteworthy point is that all four transfer functions of PSC can be modeled as a low-pass filter like the droop controller.

Figure 5.4 shows the bode results the Syn inverter. According to the Figure 5.4 Inverter has the most complex bode diagram among GFMs. The most highlightable behavior of the Syn inverter is the very sharp magnitude and angle change in a certain frequency range. This bode diagram will ensure oscillatory behavior in any disturbance. Like the PSC, the Ydq and Yqd can decrease any disturbance.

In this subsection, Nichols diagram of all GFM converters is presented. Nichols diagram is a frequency domain indicator for the transfer function. Nichols can be used for model reduction. The model reduction is necessary for dealing with multiple inverters. Nichols plots the admittance of each component with the gain and phase in the axes. The results show that the Droop GFM has the most straightforward Nichols diagram with two major sharp points in Ydd and four major sharp points in Ydq whereas the Syn inverter has

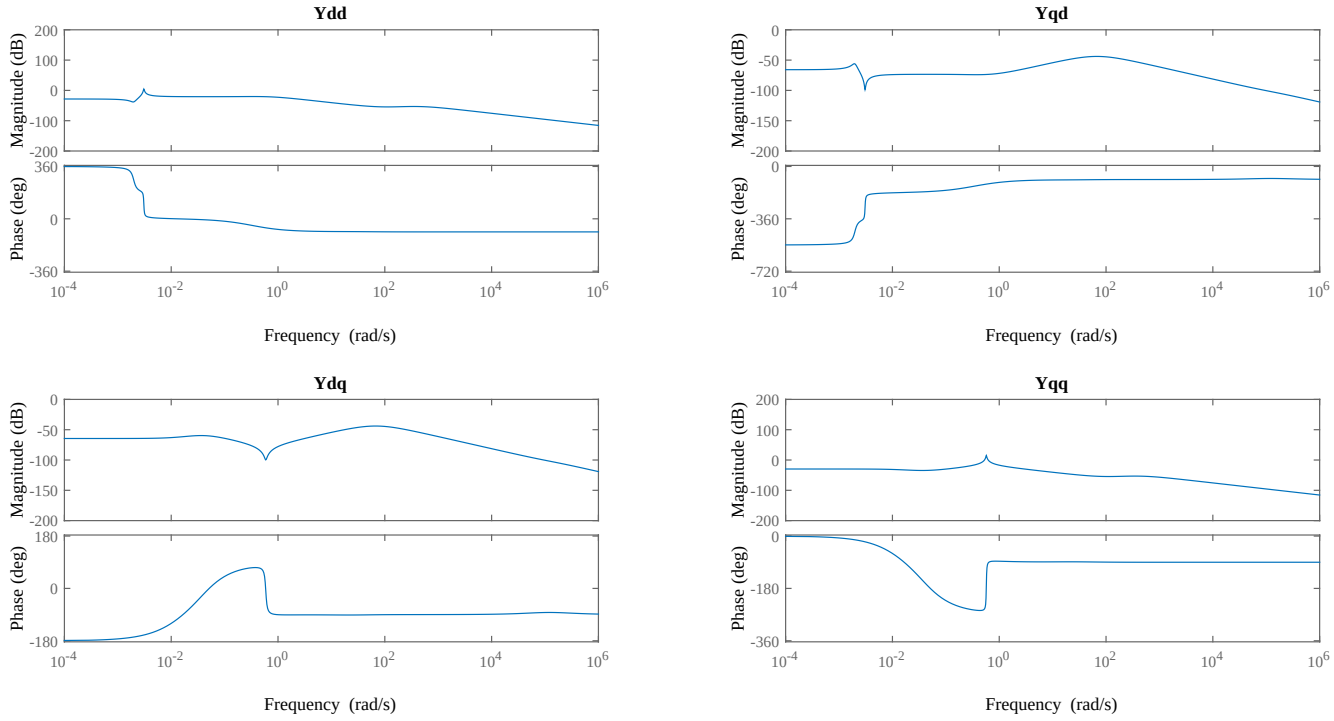

Figure 5.3: Bode diagram of PSC inverter with optimal parameters

the most complex Nichols diagram. Therefore, the Droop strategy is the easiest to make the model reduction study. Another noteworthy point is that the four transfer matrices may have very different behaviors in a specific inverter. This makes the parameter tuning very complex because all four transfer functions must be maintained in the stable margin simultaneously.

All four transfer functions have a negative gain with varying frequency for the Droop inverter. Especially in Y_{dd} with the change of frequency, the open-loop phase jumps from zero to -90^o; however, In VIL with the same parameters, all four transfer functions that have a gain of more than 0 dB. In addition, in Y_{dq}, the open-loop phase varies between 360^o and -90, which is not very well behaved. The Nichols diagram of Syn inverter, which is shown in Figure 5.7 is the most complex among other inverters. Although the results for Y_{dq} and Y_{qd} are both in the stable range, the Y_{dq} and Y_{qd} appear to behave very arbitrary and also in some points they get a positive gain in perturbation. PSC control results are shown

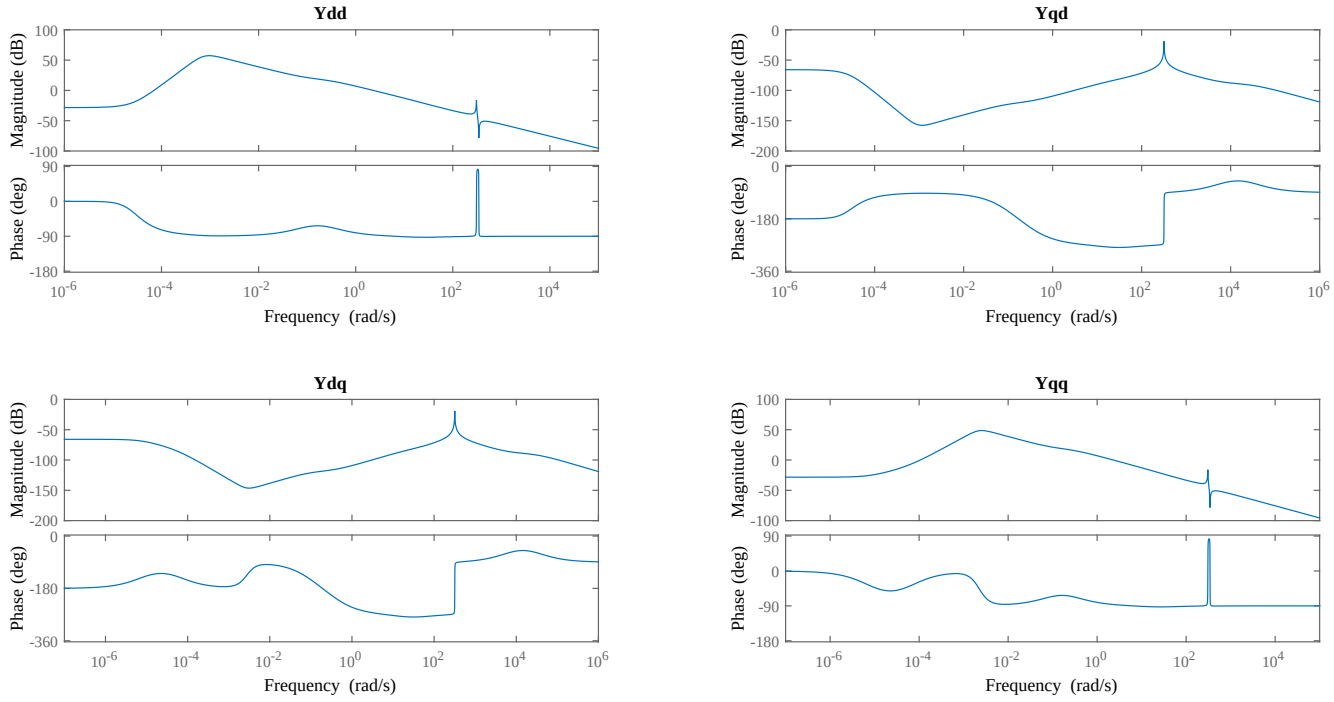

Figure 5.4: Bode diagram of Syn inverter with optimal parameters

in Figure 5.8. The behavior of the PSC is more similar to Droop with a not very complex behavior.

5.2 Parameter Sensitivity Analysis of GFL

Table 5.2: Optimal GFL Parameters

Parameter	Value	Parameter	Value	Parameter	Value
L_1	0.6	t_{del}	$1/40000$	K_{pC}	10
L_2	0.6	17	16	K_{IC}	0.1
C	0.5	K_{pQ}	100	K_{pP}	100
D	1	K_{IQ}	10	K_{IP}	10
K_{pPLL}	100	K_{IPLL}	6400	ω_c	10000

In this part of the results, sensitivity analysis is performed for the parameters mentioned in section 4.4 for the GFL. The Base stable impulse response of the GFL inverter is highlighted in Figure 5.9 and the corresponding parameters are mentioned in Table 5.2

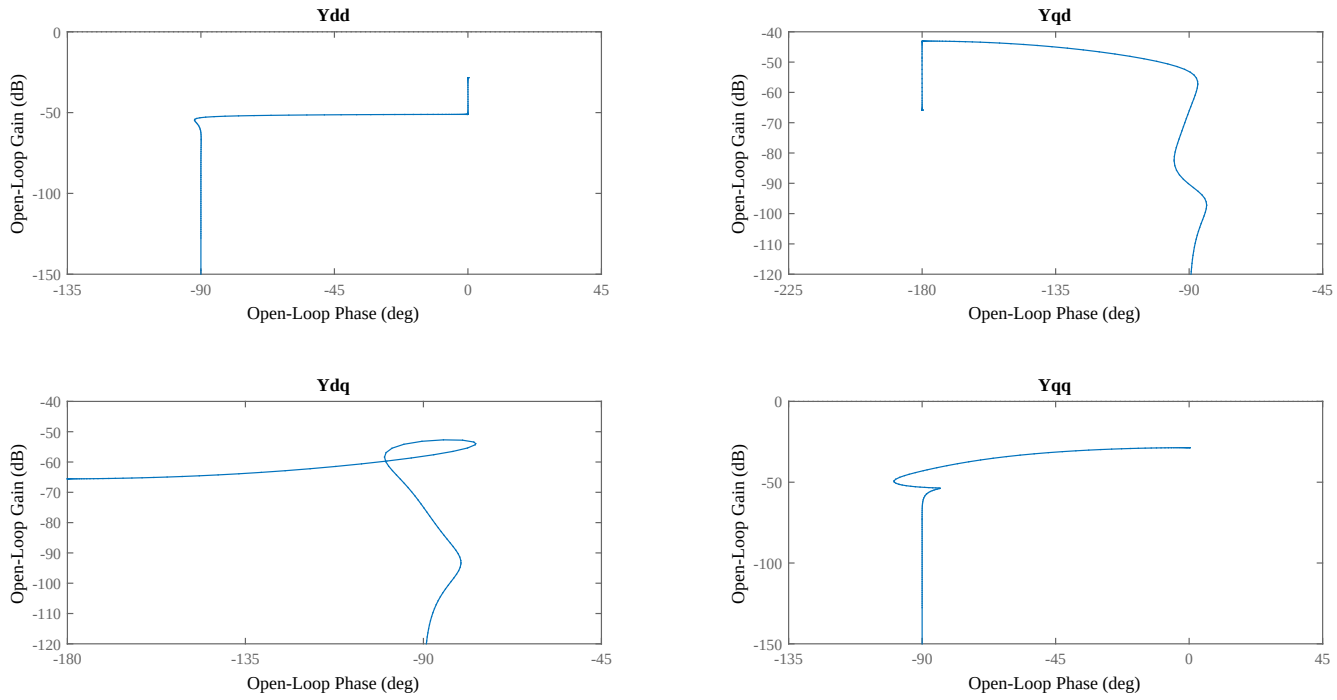

Figure 5.5: Nichols diagram of Droop GFM inverter for optimal parameters

As it can be seen in Figure 5.9, all four transfer functions result in a stable behavior, and all of the magnitudes are damped after a particular time. However, in order to better understand the effect of each important parameter in impulse behavior, sensitivity analyses are performed by repetition of simulations for different parameters.

5.2.1 steady-state Angle

The steady-state angle is the difference between local and global dq frames. In power systems, the operation angles of generators may be different. Therefore this difference must be included in inter-area oscillations. The results of changing the steady-state angle from 0 rad to 0.006 rad are presented in figs. 5.10 to 5.13.

Evaluating figs. 5.10 to 5.13 clears that there is a certain margin for θ that increasing the amount of θ more than that margin deteriorates the small signal stability, since the impulse response of Y_{qd} and Y_{qq} are converging to infinite amount. This shows that a few poles

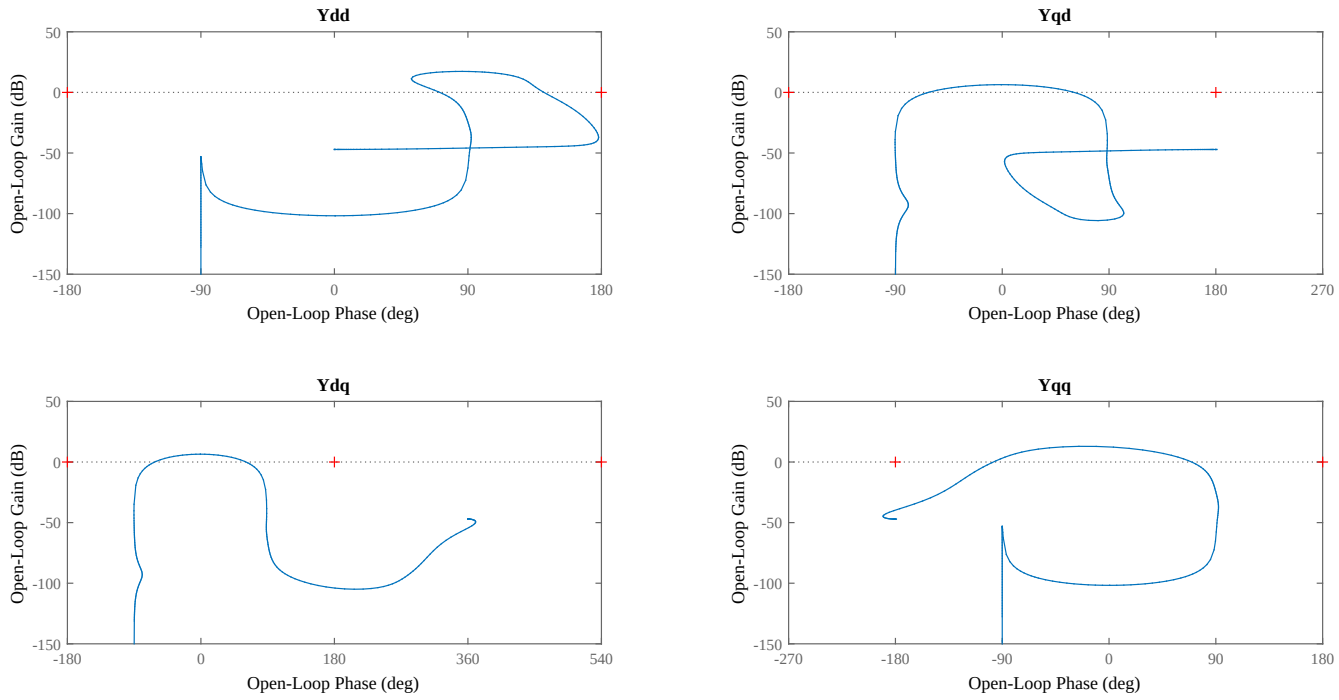

Figure 5.6: Nichols diagram of VIL inverter for optimal parameters

exist on the right side of the real axis, which drives the small signal stability of the inverter to an unstable margin. The margin of θ, in this case, is around 0.005 rad. The results are analogous to synchronous generators where the internal angle must be in a certain range generator to remain stable.

5.2.2 Current Control Block

For analyzing effect of the current loop, amount of the proportional gain (K_{pc}) is decreased from 100 to 0.1, as shown in figs. 5.14 to 5.16. Comparing the obtained results shows that changing K_{pc} to 10 improves the impulse response, by reducing the overshoot of Y_{qd} and Y_{qq}. However, The analysis shows that reducing the amount of K_{pc} to 0.01 drives the inverter to unstable margin. So, this amount is fixed to 10. Subsequently, the integral gain (K_{Ic}) of the current control loop is increased from 0.1 to 10, which is illustrated in fig. 5.17. Comparing both figures unfolds that this change will decrease the overshoot of Y_{dq} and Y_{qq}

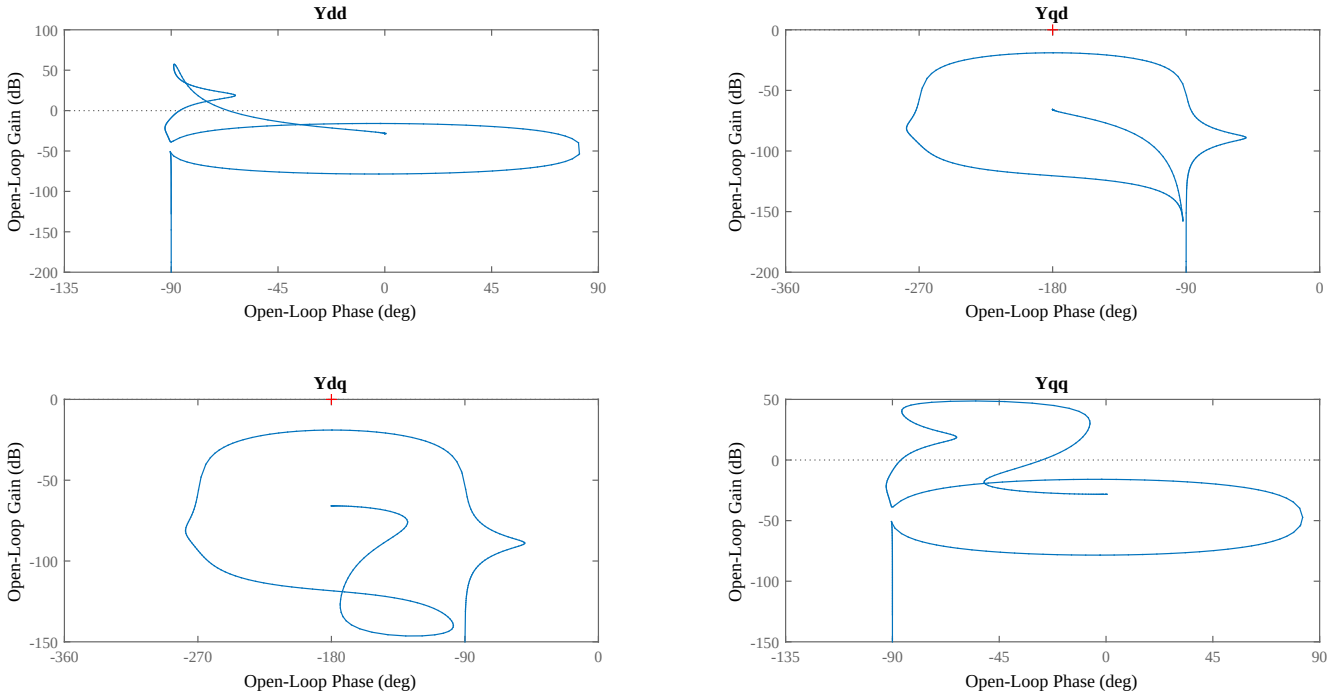

Figure 5.7: Nichols diagram of Syn inverter for optimal parameters

from both 6000 to less than 5000 and 3000 P.u respectively. Therefore $K_{Ic} = 10$ is a better selection.

5.2.3 Power Control Block

The impact of the proportional gain of active and reactive power (K_{pP} and K_{pQ}) is analyzed by diminishing its amount from 100 to 10, which is depicted in Figure 5.19. The obtained results show that, while the overshoot of Y_{dq} and Y_{qq} is reduced, the dynamic response speed is deteriorated compared to Figure 5.9.

Then, the integral gain of active and reactive power (K_{IP} and K_{IQ}) is reduced to 1 from 10. The results are shown in Figure 5.20, which has a slower settling time in case of Y_{qd} compared to Figure 5.9.

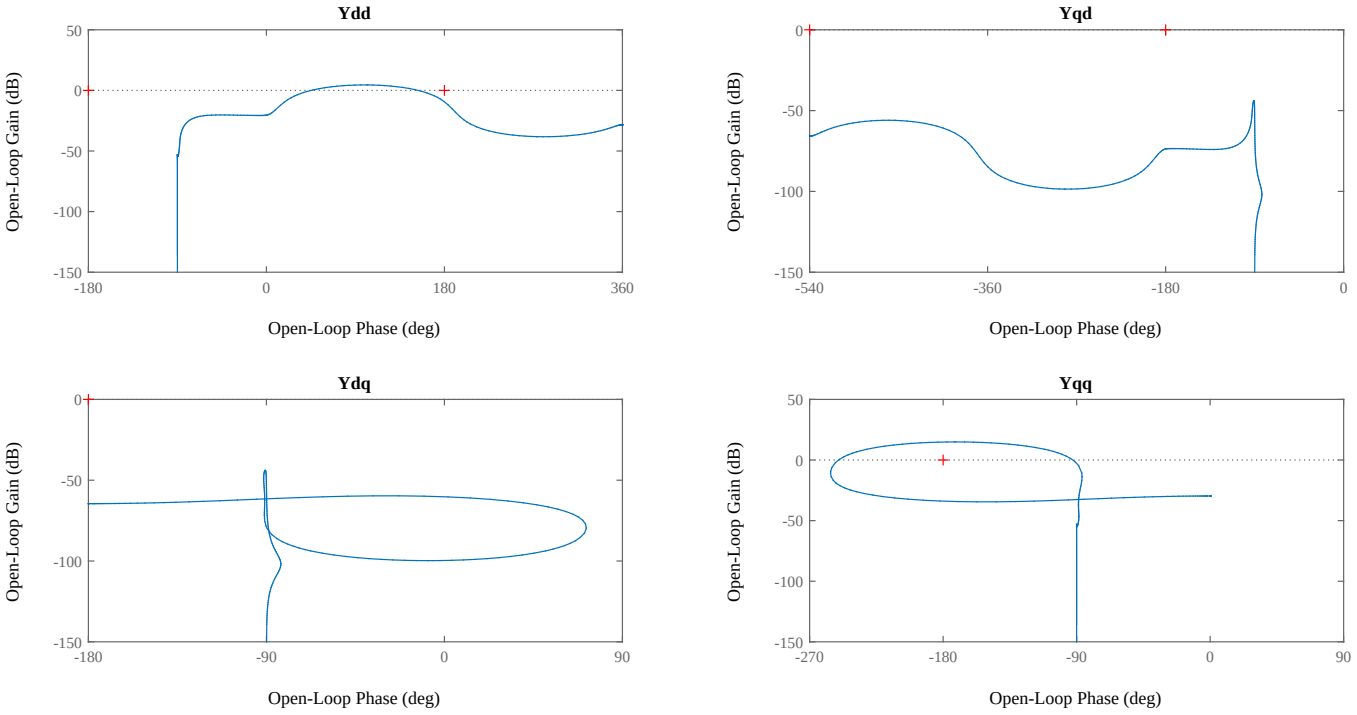

Figure 5.8: Nichols diagram of PSC inverter for optimal parameters

5.2.4 PLL Block

The proportional and integral gains of PLL block (K_{pPLL}, K_{IPLL}) can have an impact on the small signal stability of the grid-following inverters. First, the effect of the K_{pPLL} is evaluated by setting its value to 1000, which is shown in Figure 5.21. Comparing Figure 5.21 with Figure 5.9 shows that there is no difference between these two results. So, it can be concluded that the amount of K_{pPLL} is not effective in the case of a GFL inverter.

Secondly, the impact of K_{IPLL} is measured by setting it to 640. The result is depicted in Figure 5.22, and it shows that this change has reduced the overshoot of Y_{dq} and Y_{qq} considerably compared to Figure 5.9, however the settling time has become slower.

For further analysis, the amount of K_{IPLL} is set to 10000, which is shown in Figure 11. As it is visible unlike the settling time, the overshoot amount is deteriorated. So, it can be concluded that speed of settling time has direct proportion with the amount of K_{IPLL},

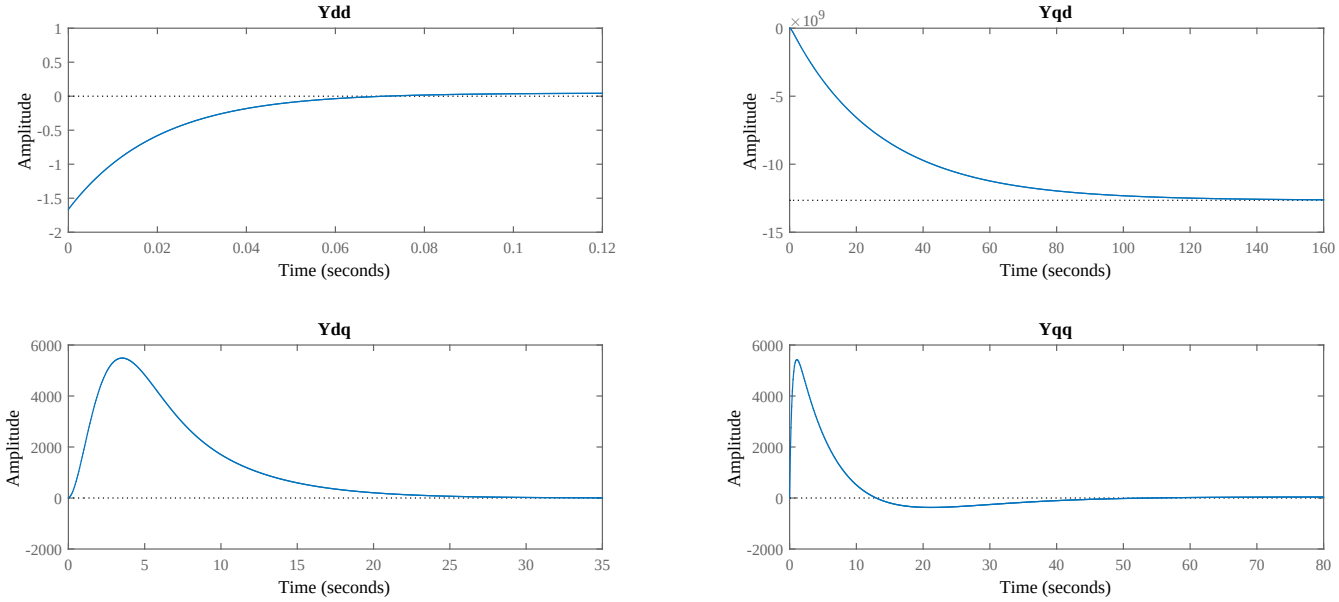

Figure 5.9: Basic impulse response for tuned parameters of GFL.

which is inverse in case of overshoot.

5.2.5 Output Filter

For further analysis, the values of L1 and L2 filters are decreased to 0.1 p.u., and the results are shown in Figure 5.24. Compared to Figure 5.9, this change only reduced the overshoot amount of Y_{dq}. Then, these values are set to 1 p.u. for one more analysis. The results are reported in Figure 5.25, which only differs from Figure 5.24 and Figure 5.9 in terms of the Y_{dq} overshoot.

Finally, the value of the capacitor is changed to 1 p.u. for observing its impact in Figure 5.26. Evaluating the result did not show any difference. Hence, it can be concluded that the capacitor filter does not affect the response of the inverter, at least in this range.

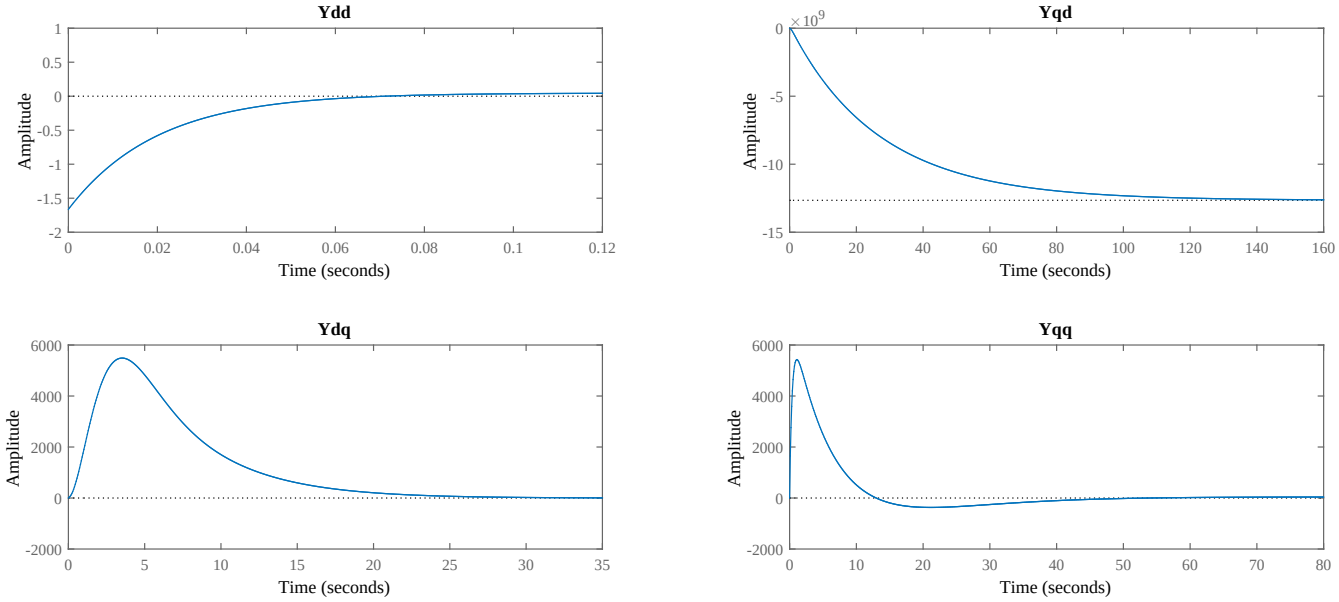

Figure 5.10: GFL impulse response for $\theta = 0$.

5.3 Conclusion

Among GFMs, the Synchronvertor strategy seemed to be the most complex and challenging to undergo a model reduction. While droop control seemed well behaved, other strategies could not provide stable results with the same parameters. In GFLs, Y_{dq} is observed to be more prone to instability than the other three transfer functions. Also, steady-state angle, K_{IPLL}, and K_{Pc} were observed to be more dominant parameters in system stabilizing. In the same manner, a steady-state angle margin for stability is derived for GFL, which is analogous to internal angle stability in a synchronous generator.

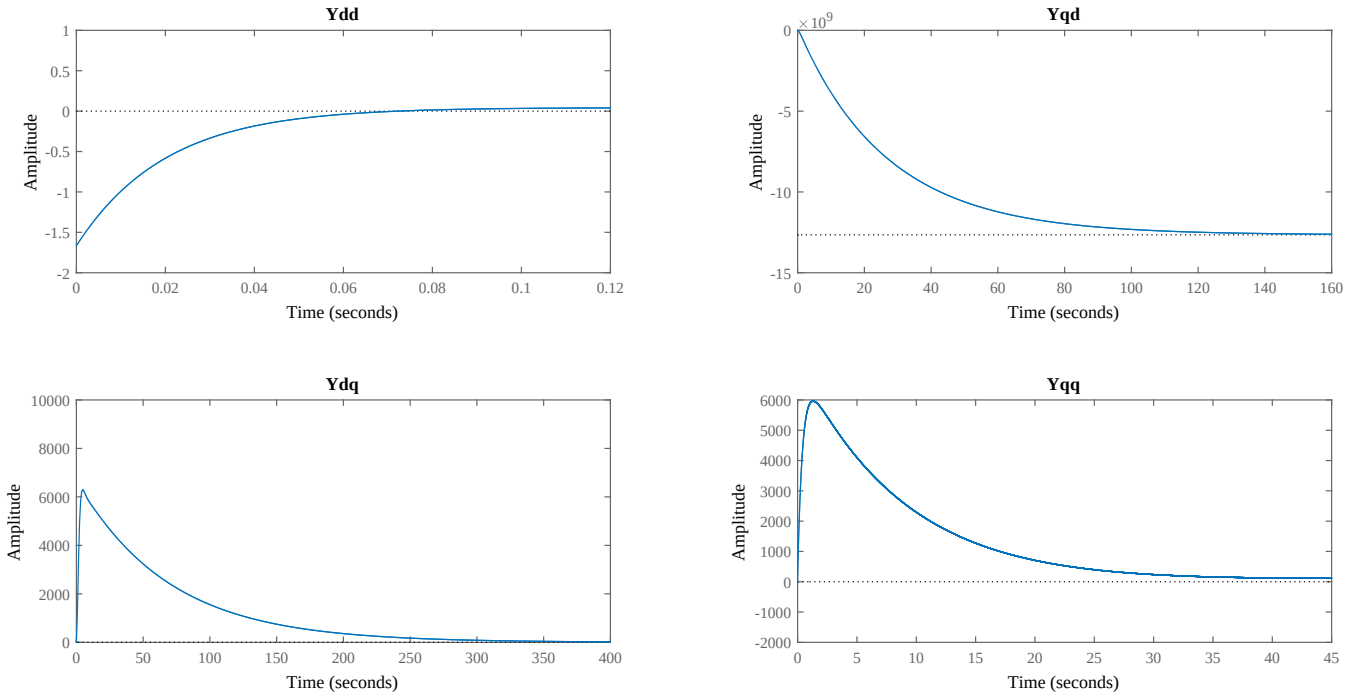

Figure 5.11: GFL impulse response for $\theta = 0.004$.

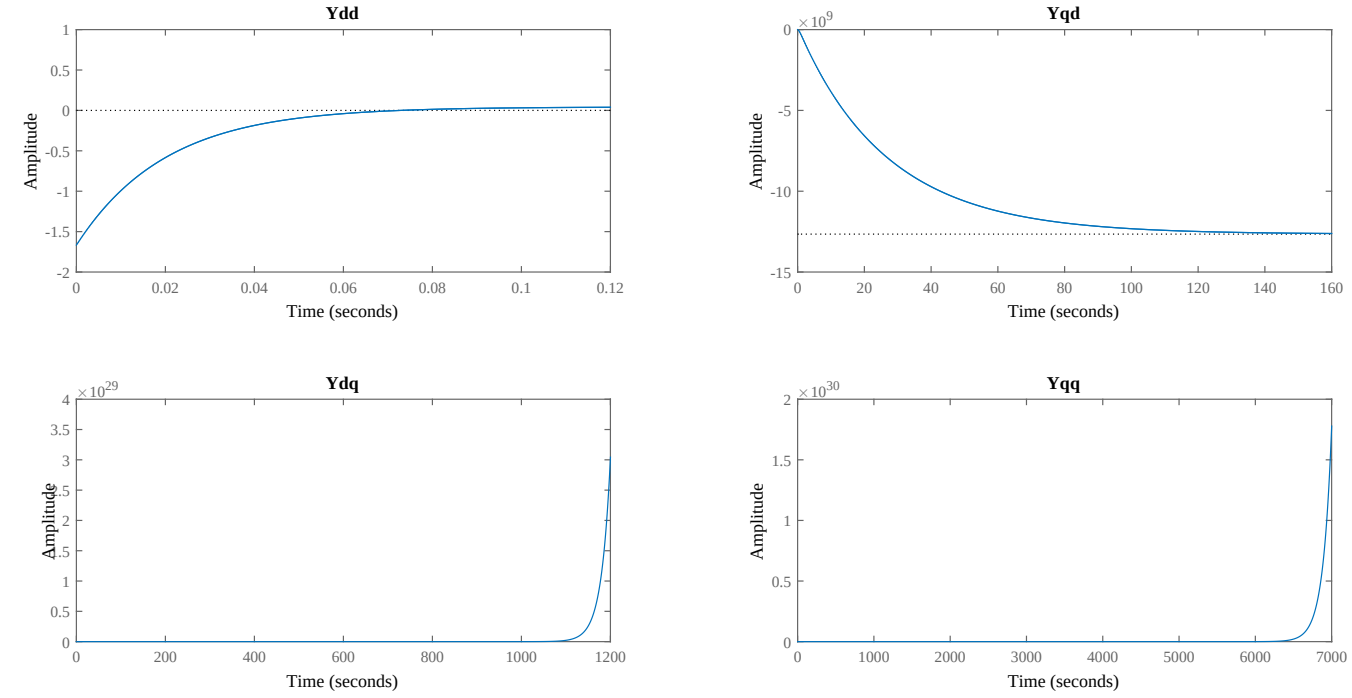

Figure 5.12: GFL impulse response for $\theta = 0.006$.

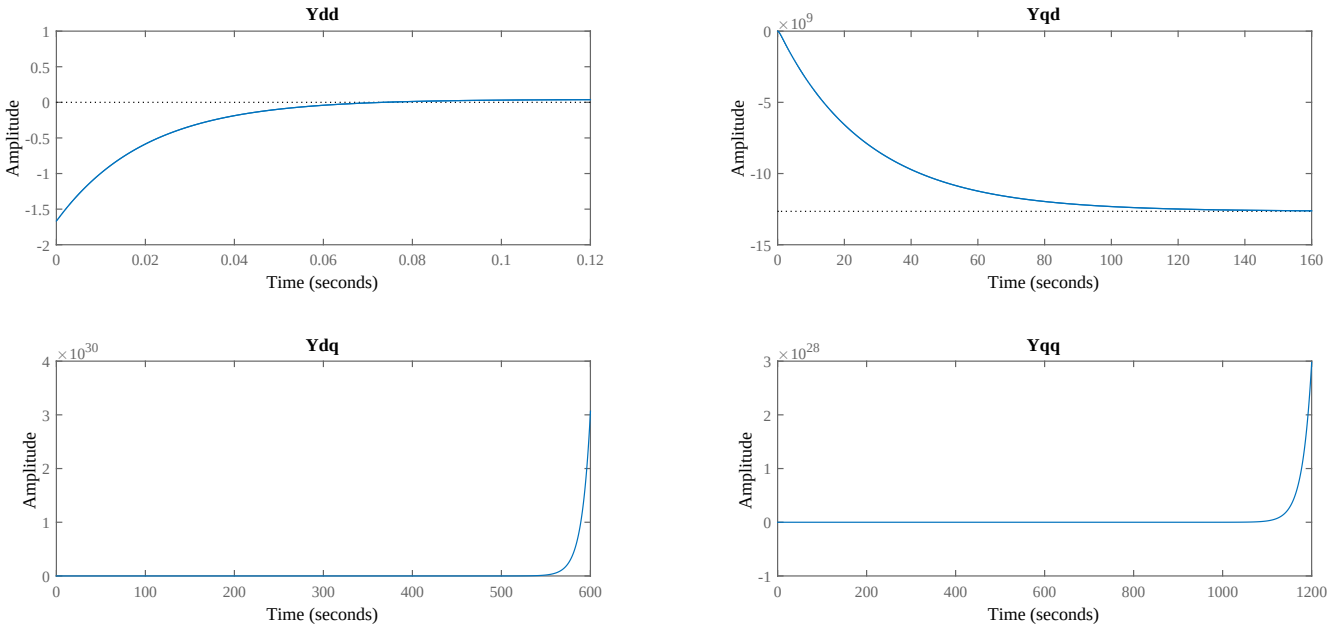

Figure 5.13: GFL impulse response for $\theta = 0.008$.

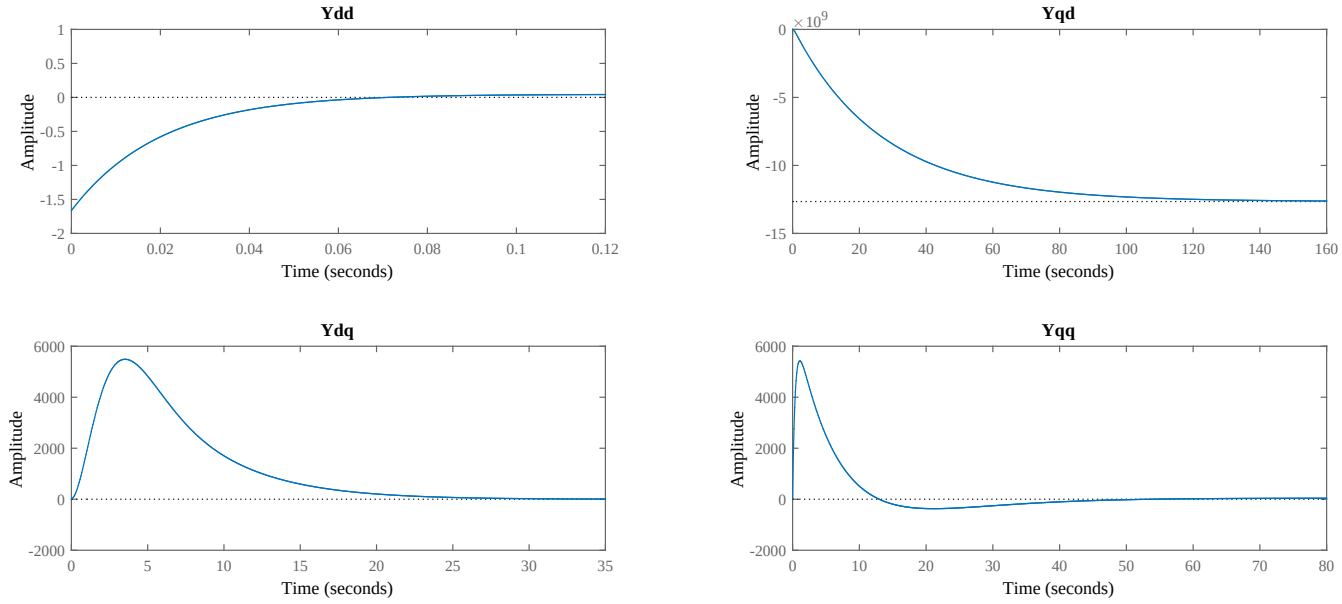

Figure 5.14: GFL impulse response for $K_{PC} = 100$.

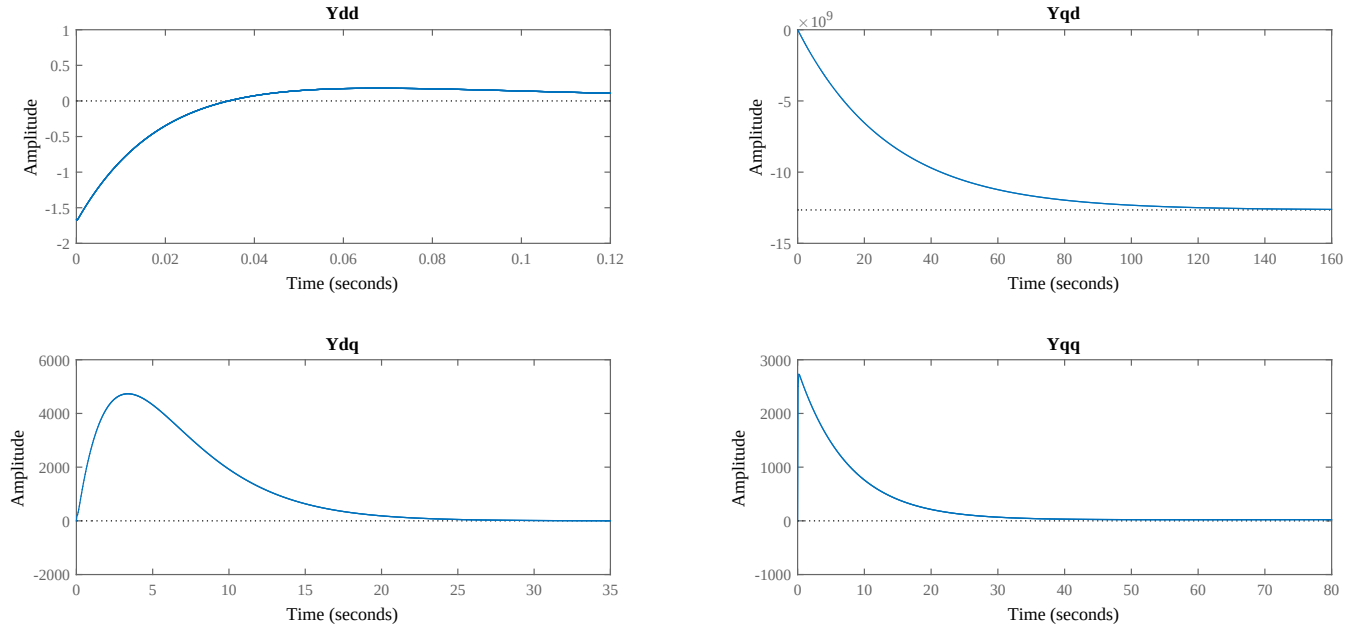

Figure 5.15: GFL impulse response for $K_{PC} = 10$.

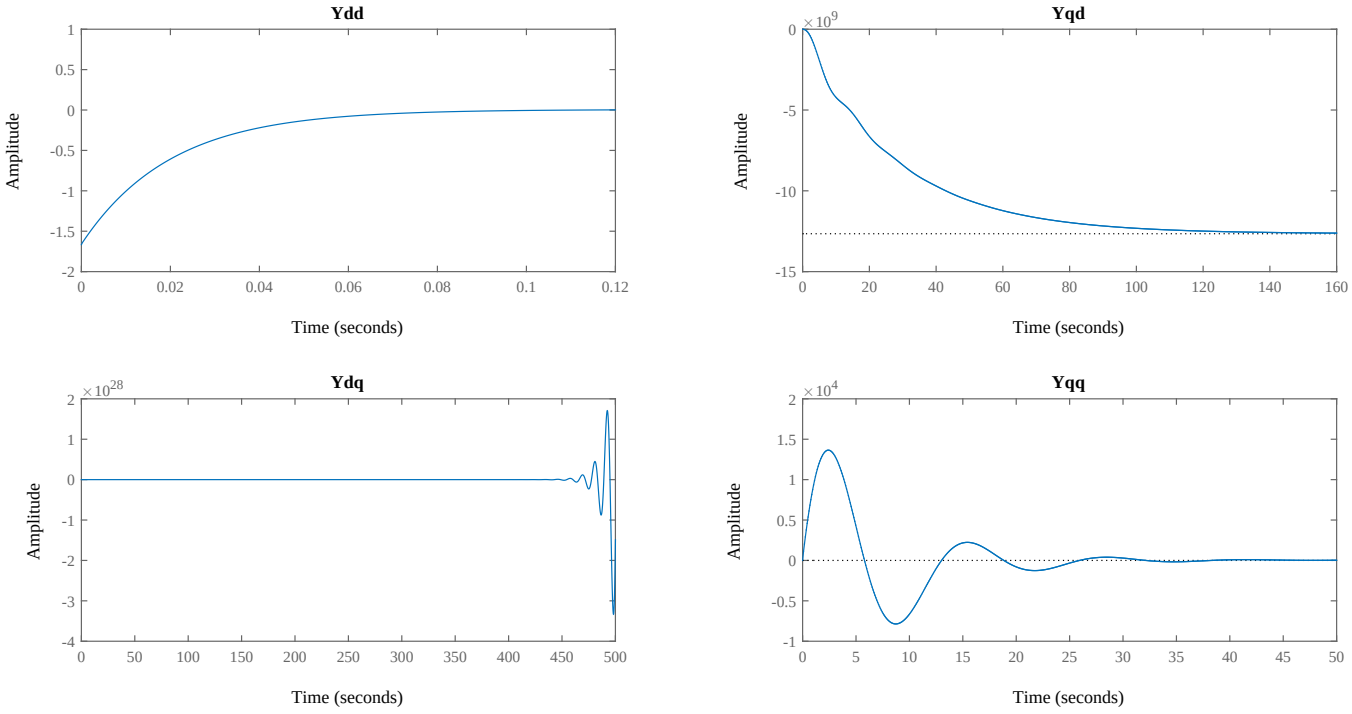

Figure 5.16: GFL impulse response for $K_{PC} = 0.1$.

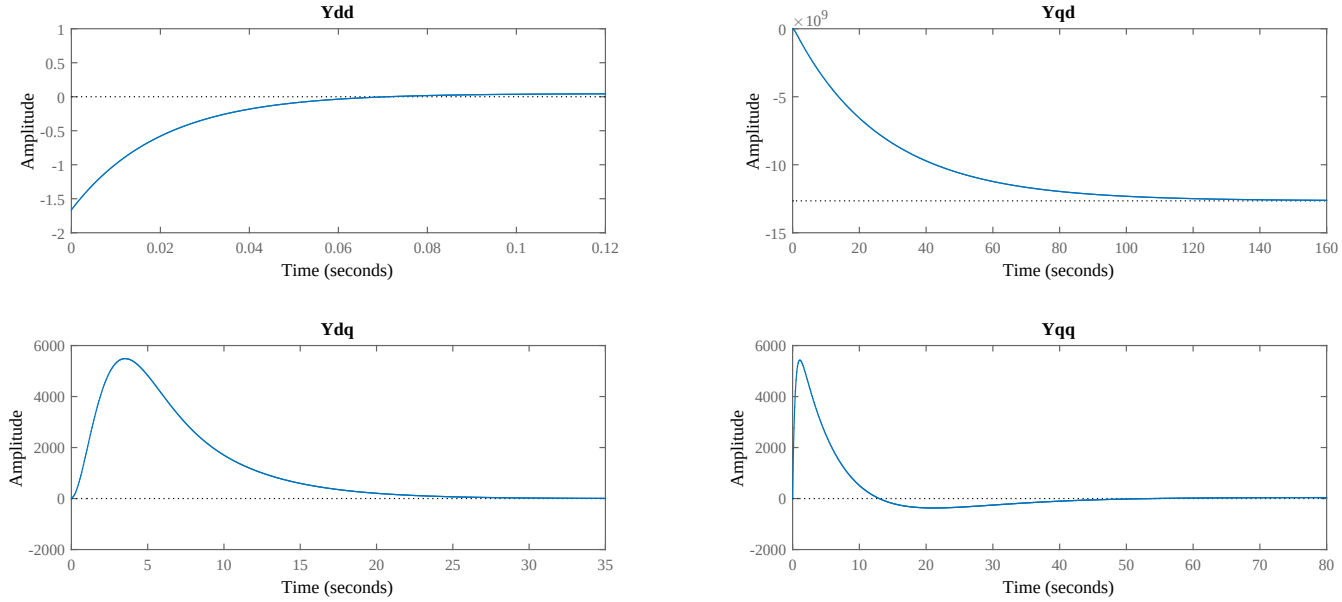

Figure 5.17: GFL impulse response for $K_{Ic} = 0.1$.

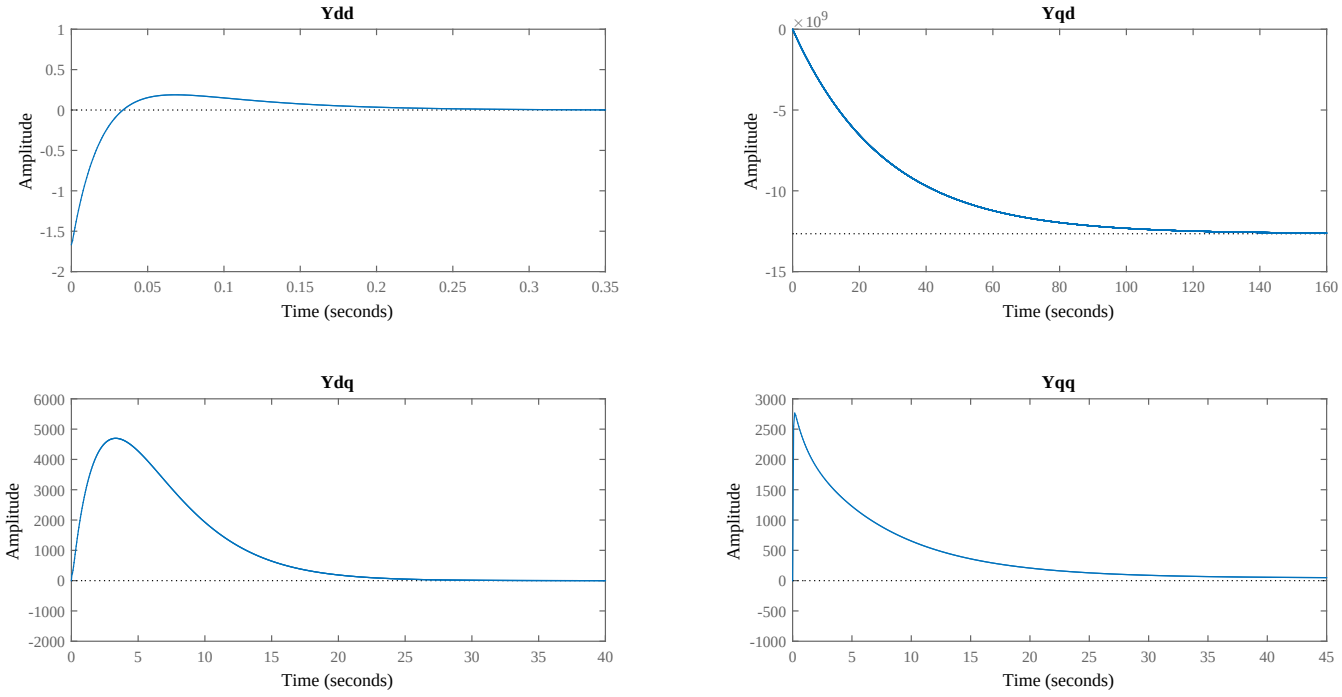

Figure 5.18: GFL impulse response for $K_{Ic} = 10$.

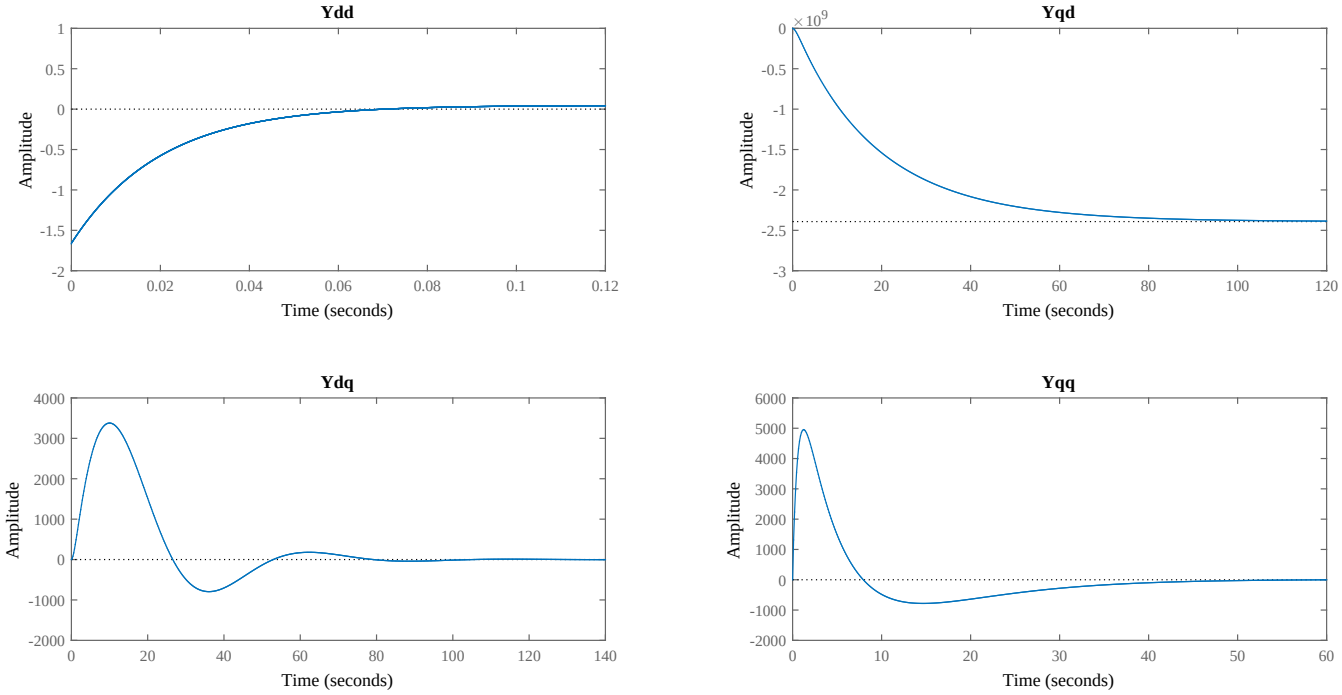

Figure 5.19: GFL impulse response for $K_{pP} = 10$ and $K_{pQ} = 10$.

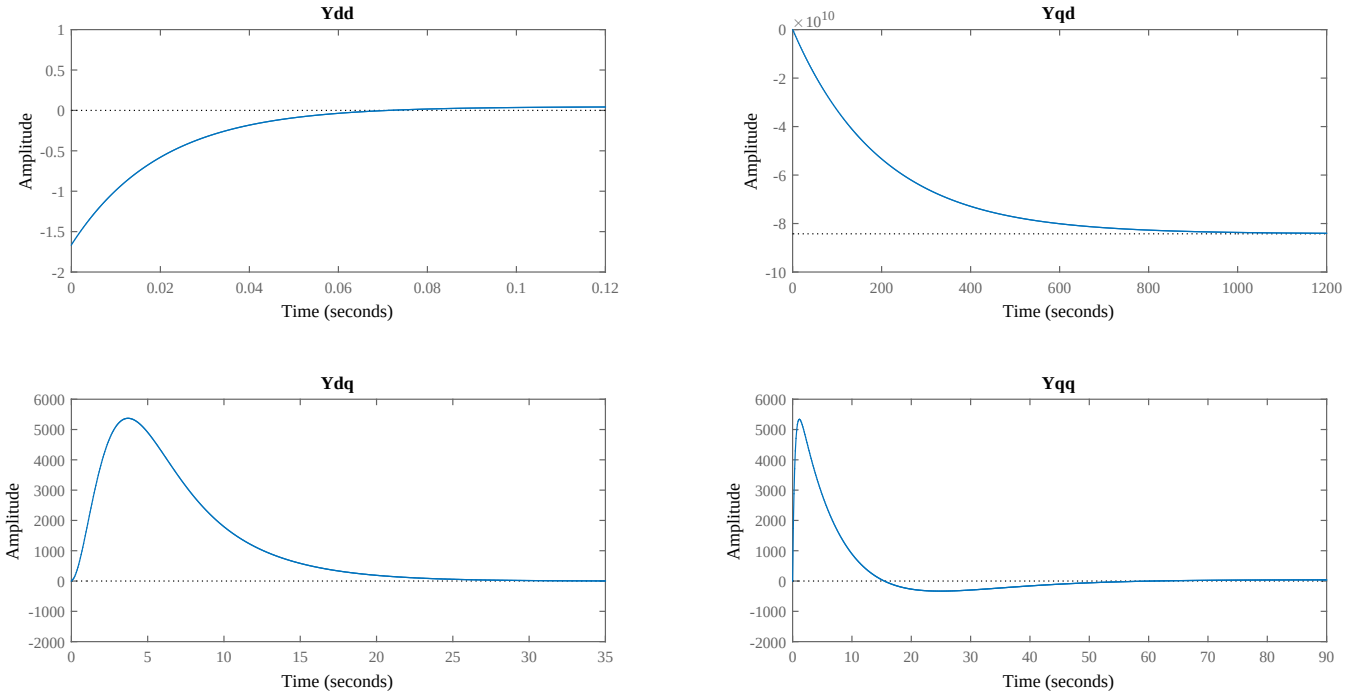

Figure 5.20: GFL impulse response for $K_{IP} = 1$ and $K_{IQ} = 1$

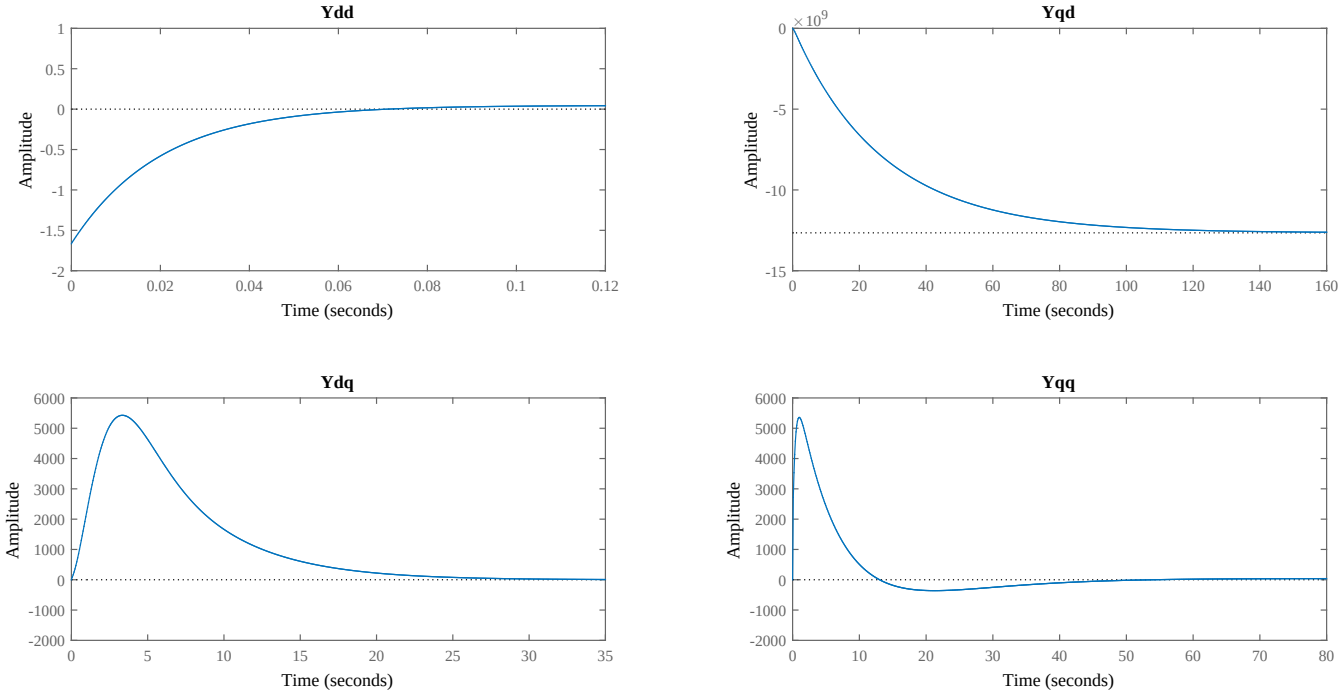

Figure 5.21: GFL impulse response for $K_{PPLL} = 1000$.

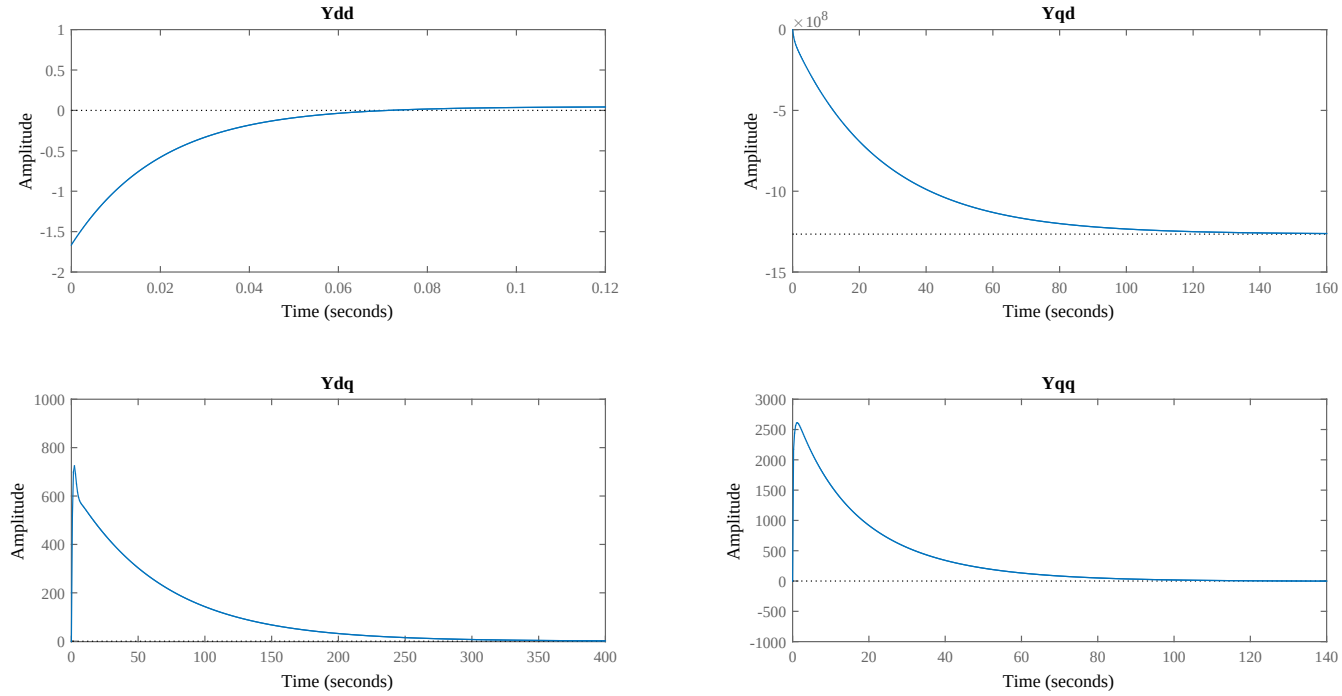

Figure 5.22: GFL impulse response for $K_{IPLL} = 640$.

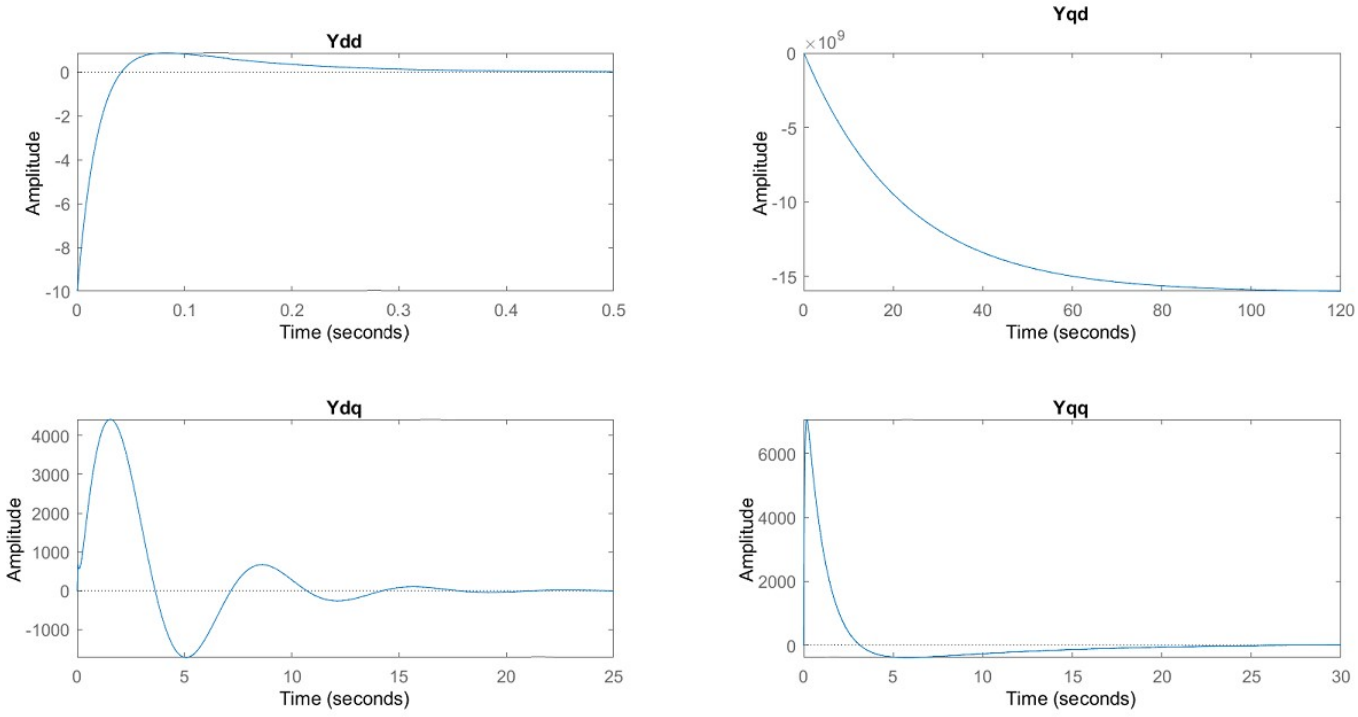

Figure 5.23: GFL impulse response for $K_{IPLL} = 10000$.

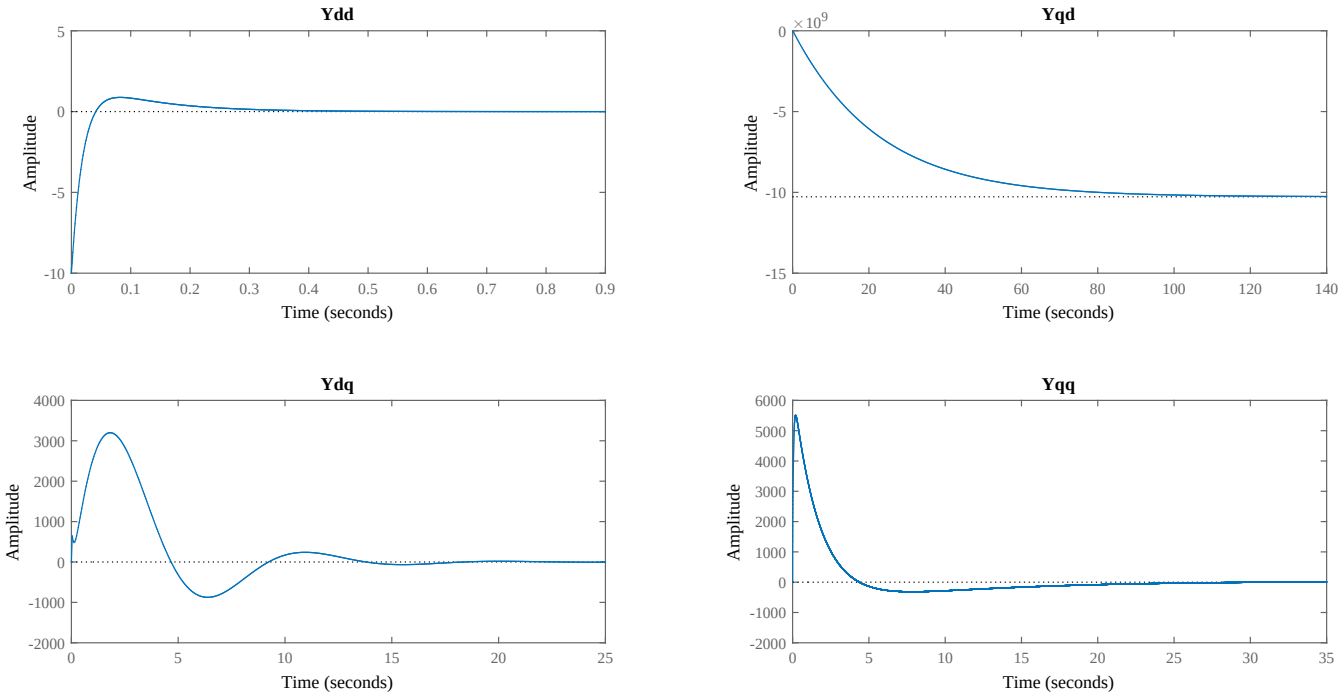

Figure 5.24: GFL impulse response for $L_1 = 0.1$ and $L_2 = 0.1$.

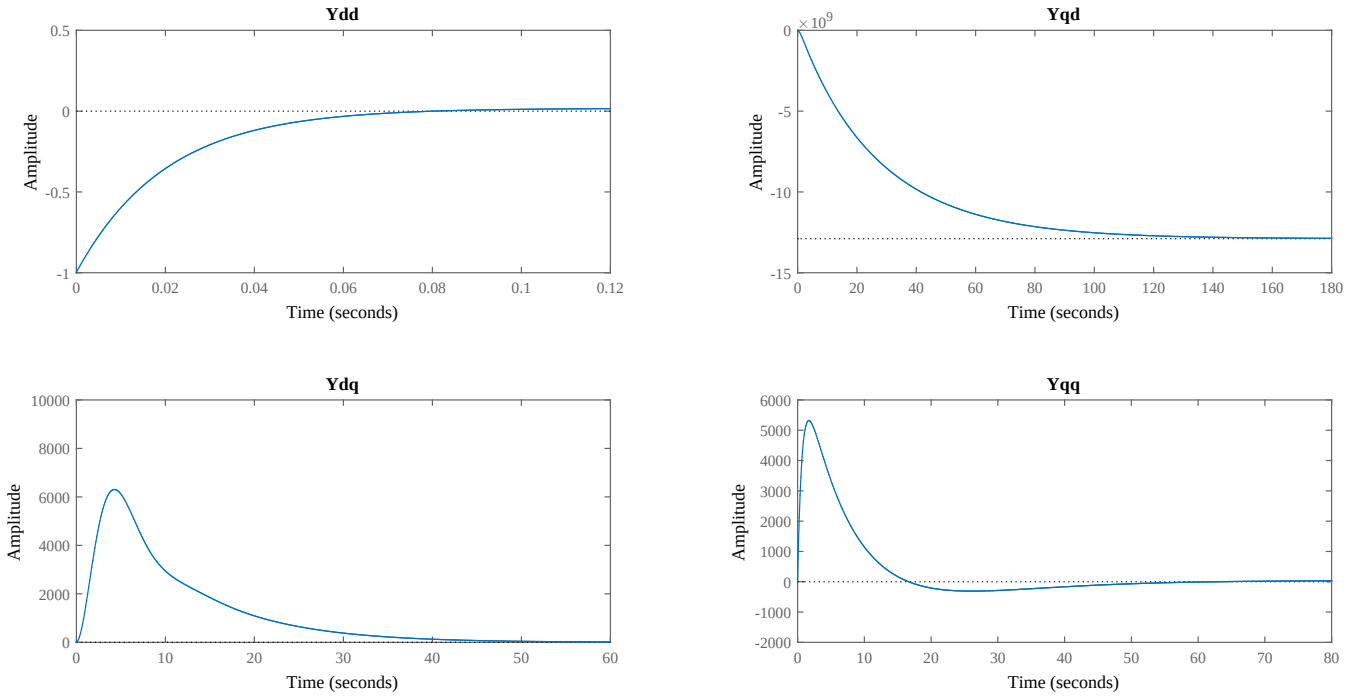

Figure 5.25: GFL impulse response for $L_1 = 1$ and $L_2 = 1$.

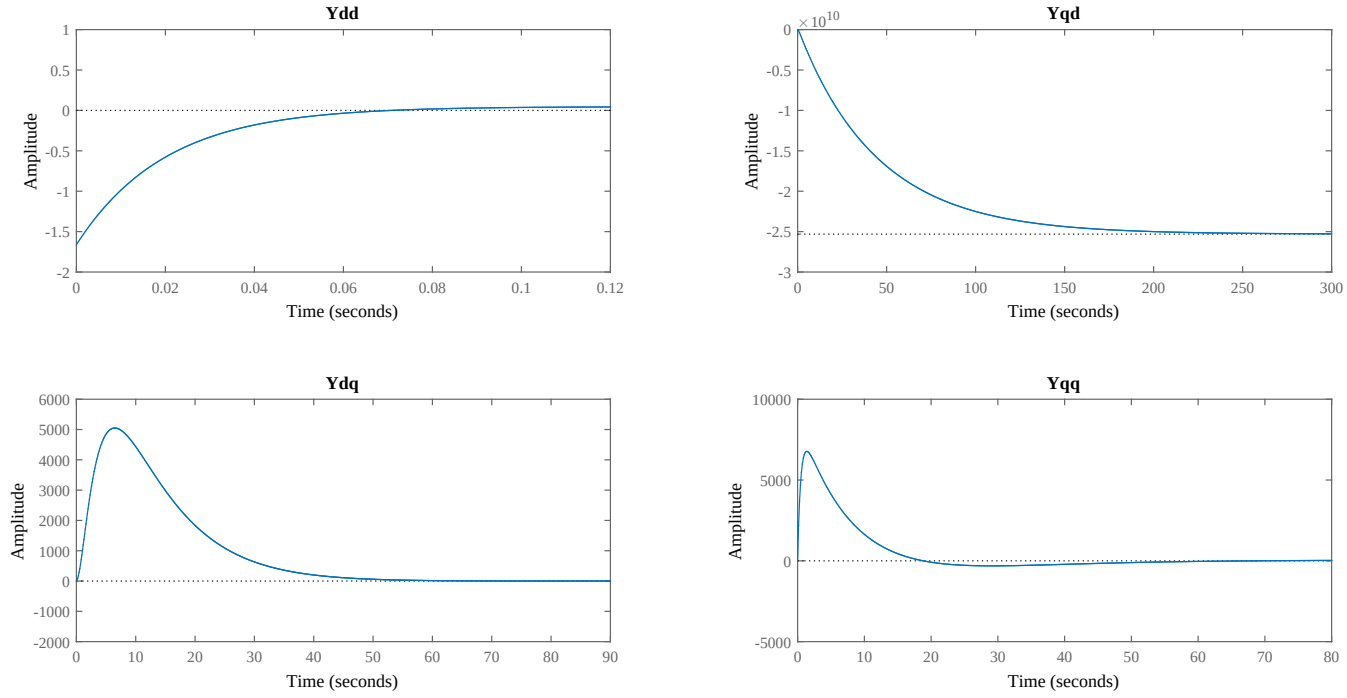

Figure 5.26: GFL impulse response for $C = 1$.

CHAPTER 6
CONCLUSION

In this last chapter, the thesis has been concluded and also future research steps are presented.

6.1 Contributions

An exact small-signal study of inverters with different control strategies is necessary for inter-area oscillations and stability analyses in power systems. However, the Small-signal modelings of inverters studied in the literature, are limited due to stand-alone consideration of inverter, lack of proper consideration of propagation of small-signal disturbance through power loop, DC-side dynamics, and most importantly, consideration of global and local dq frame differences due to power flow which is particularly a property of large power grids. The contribution of the proposed thesis is summarized as follows:

Due to the complexity and non-linearity and a coupled control framework in the dq frame, a systematic method should be used to simplify the inverter equations. In this regard, a matrix formulation of d and q components is proposed, and every block is presented as a 2×2 matrix. The matrix formulation can handle dq- coupled control blocks and also help to formulate linearized forms of non-linear blocks such as power measurement, DC dynamics, droop, and PLL. In addition, the matrix formulation of each block reduces the system equations to algebraic equations with the order of one. This reduction is crucial in exact inverter modeling because a presentable explicit equation can be derived for the output admittance/impedance in small-signal by solving the set of equations. In order to tackle solving a set of equations with a size of 16×16, a computational symbolic solver (MATLAB) is used. This implementation makes post-processing easier so that each block term in the admittance/impedance model can be readily replaced with its 2×2 components. After

the replacement process, a 2×2 admittance/impedance is derived. Then each term forms a transfer function that indicates the propagation dynamics of a small-signal perturbance in the inverter. The parametric derivation of exact inverter output admittance/impedance is the contribution of this thesis because it will be a basis for accurate sensitivity analysis of parameters and their importance in system stability.

Six inverter types are chosen as GFL-basic, GFL-PLL, GFM-droop, GFM-Virtual Inertia, GFM-Power Synchronization Control, and GFM-synchronvertor to be studied. The previous approaches only included either GFL or GFM with a droop or virtual inertia control strategy. In addition, the generation of power signal requires both voltages and currents and a low-pass filter formulated in matrix form. In addition, both currents and voltage are outputs of a dq/abc transform which is affected by the angle perturbation. abc/dq transform in the modulation index also is affected by the angle perturbation. The angle perturbation in the GFL is generated via PLL's small-signal block and exists in the literature, whereas the angle perturbation of GFMs is considered to be zero. However, the angle generation in all of the mentioned GFM inverters is generated via feedback from output power which itself is affected by angle perturbation via both voltage and current abc/dq blocks. Consideration of this new loop is a contribution of this work that has a significant effect on the GFM stability.

In the chapter 5, first, all inverters are compared in terms of eigenvalues, time domain, and frequency domain responses for given parameters, and their results are discussed. Results show considerable complexity in the GFM formulation and stability issues, especially the syncronvertor strategy, compared with the acceptable performance of GFL. Finally, sensitivity analyses are performed for selected parameters to obtain the most effective elements in the low-frequency oscillations. According to the results, one of the significant parameters acting in stability is steady current loop gain. The parameters, such as current loop integral gain and PLL gains, can have an effect on the settling time and stability of dq admittance. It is also observed that the dq admittance is the first component of an inverter

that gets unstable.

Another highlight of the results is that there is a narrow stability margin for the steady-state angle difference between global and local dq frames caused by the load flow difference of inverters. This observation is analogous to the angle stability of synchronous generators. As a result, the same approach for analysis of critical angle and critical time in synchronous generators can also be theorized for inverter-based grids.

6.2 Future research

This study is suitable for small-signal and low-frequency phenomena such as inter-area oscillations, and considers all block diagrams in an inverter; therefore, the resultant transfer functions may have 16 to 23 poles (eigenvalues). One direction for future research can be reducing the transfer function to a lower order model, probably with a least square curve fitting in the Nichols diagram, to make the analysis of inter-area oscillation in multiple inverter systems easier. Another direction can be extending the study in a large-signal environment and including the current limiter block in the studies. Finally, another extension may consider active power-sharing and oscillatory voltage control methods as inverter control strategies.

REFERENCES

[1] M. Saeedifard, S. Meliopoulos, and S. Lotfifard, "Grid supporting controllers for enabling 100% penetration of inverter based resources," *PSERC Proposal*, no. S90, p. 1, 2019.

[2] "General introduction to electromagnetic transient simulations - mathematical background and common applications," *PSCAD Webinar*, p. 30, 2020.

[3] H. W. Dommel, "Digital computer solution of electromagnetic transients in single- and multiphase networks," *IEEE Transactions on Energy Conversion*, vol. PAS-88, no. 4, pp. 388–399, 1969, doi:10.1109/TPAS.1969.292459.

[4] H. W. Dommel, "Nonlinear and time-varying elements in digital simulation of electromagnetic transients," *IEEE Transactions on Power Apparatus and Systems*, vol. PAS-90, no. 6, pp. 2561–2567, 1971, doi:10.1109/TPAS.1971.292905.

[5] Y. Xu, Y. Chen, L. Chen, and S. Mei, "Integrating an improved averaged model for pwm converters into emtp," *IEEE Transactions on Power Delivery*, vol. 29, no. 1, pp. 291–293, 2014, doi:10.1109/TPWRD.2013.2248958.

[6] J. Rupasinghe, S. Filizadeh, and L. Wang, "A dynamic phasor model of an mmc with extended frequency range for emt simulations," *IEEE Journal of Emerging and Selected Topics in Power Electronics*, vol. 7, no. 1, pp. 30–40, 2019.

[7] T. Yang, "Development of dynamic phasors for the modelling of aircraft electrical power systems," Ph.D. dissertation, The University of Nottingham, 2013.

[8] Y. Amran, F. Huliehel, and S. Ben-Yaakov, "A unified spice compatible average model of pwm converters," *IEEE Transactions on Power Electronics*, vol. 6, no. 4, pp. 585–594, 1991, doi:10.1109/63.97756.

[9] P. Pourbeik *et al.*, "Generic dynamic models for modeling wind power plants and other renewable technologies in large-scale power system studies," *IEEE Transactions on Energy Conversion*, vol. 32, no. 3, pp. 1108–1116, 2017.

[10] M. Klein, G. Rogers, and P. Kundur, "A fundamental study of inter-area oscillations in power systems," *IEEE Transactions on Power Systems*, vol. 6, no. 3, pp. 914–921, 1991.

[11] L. Ding, X. Lu, and J. Tan, "Comparative small-signal stability analysis of grid-forming and grid-following inverters in low-inertia power systems," in *IECON 2021 – 47th Annual Conference of the IEEE Industrial Electronics Society*, 2021, pp. 1–6.

[12] L. Harnefors, M. Bongiorno, and S. Lundberg, "Llight harvesting," *IEEE Transactions on Industrial Electronics*, vol. 3, no. 10, p. 763, 2011, doi:10.1038/nchem.1145.

[13] X. Wang, L. Harnefors, and F. Blaabjerg, "Unified impedance model of grid-connected voltage-source converters," *IEEE Transactions on Power Electronics*, vol. 33, no. 2, pp. 1775–1787, 2018.

[14] B. Wen, D. Boroyevich, R. Burgos, P. Mattavelli, and Z. Shen, "Analysis of d-q small-signal impedance of grid-tied inverters," *IEEE Transactions on Power Electronics*, vol. 31, no. 1, pp. 675–687, 2016, doi:10.1109/TPEL.2015.2398192.

[15] C. Yang, L. Huang, H. Xin, and P. Ju, "Placing grid-forming converters to enhance small signal stability of pll-integrated power systems," *IEEE Transactions on Power Systems*, vol. 36, no. 4, pp. 3563–3573, 2011, doi:10.1109/TPWRS.2020.3042741.

[16] A. Tayyebi, D. Groß, A. Anta, F. Kupzog, and F. Dörfler, "Frequency stability of synchronous machines and grid-forming power converters," *IEEE Journal of Emerging and Selected Topics in Power Electronics*, vol. 8, no. 2, pp. 1004–1018,

[17] R. Rosso, X. Wang, M. Liserre, X. Lu, and S. Engelken, "Grid-forming converters: Control approaches, grid-synchronization, and future trends—a review," *IEEE Open Journal of Industry Applications*, vol. 2, pp. 93–109, 2021.

[18] T. Qorai, F. Gruson, F. Colas, X. Guillaud, M.-S. Debry, and T. Prevost, "Tuning of cascaded controllers for robust grid-forming voltage source converter," in *2018 Power Systems Computation Conference (PSCC)*, IEEE, 2018, p. 8.